Atmospheric
Chemistry
and Physics
Discussions

1   **Seasonal differences in formation processes of oxidized organic aerosol near**

2   **Houston, TX**

3   Qili Dai[1, 2], Benjamin C. Schulze[2, 3], Xiaohui Bi[1, 2], Alexander A.T. Bui[2], Fangzhou Guo[2], Henry

4   W. Wallace[2, 4], Nancy P. Sanchez[2], James H. Flynn[5], Barry L. Lefer[5, 6], Yinchang Feng[1*], Robert

5   J. Griffin[2, 7]

6   [1] State Environmental Protection Key Laboratory of Urban Ambient Air Particulate Matter Pollution

7   Prevention and Control, College of Environmental Science and Engineering, Nankai University, Tianjin

8   300350, China

9   [2] Department of Civil and Environmental Engineering, Rice University, Houston, TX, 77005

10   [3] Now at Department of Environmental Science and Engineering, California Institute of Technology,

11   Pasadena, CA, 91125

12   [4] Now at Washington State Department of Ecology, Lacey WA, 98503

13   [5] Department of Earth and Atmospheric Sciences, University of Houston, Houston, TX, 77004

14   [6] Now at Division of Tropospheric Composition, NASA, Washington, DC 20024

15   [7] Department of Chemical and Biomolecular Engineering, Rice University, Houston, TX, 77005

16

17   [*]Corresponding author: Yinchang Feng (fengyc@nankai.edu.cn)

18

Atmospheric
Chemistry
and Physics
Discussions

Open Access

EGU

19   **Abstract**

20   Submicron aerosol was measured to the southwest of Houston, Texas during winter and

21   summer 2014 to investigate its seasonal variability. Data from a high-resolution time-of-flight

22   aerosol mass spectrometer (HR-ToF-AMS) indicated that organic aerosol (OA) was the largest

23   component of non-refractory submicron particulate matter (NR-PM$_1$) (on average, $46 \pm 13\%$

24   and $55 \pm 18\%$ of the NR-PM$_1$ mass loading in winter and summer, respectively). Positive

25   matrix factorization (PMF) analysis of the OA mass spectra demonstrated that two classes of

26   oxygenated OA (less and more-oxidized OOA, LO and MO) together dominated OA mass in

27   summer (77%) and accounted for 42% of OA mass in winter. The fraction of LO-OOA (out of

28   total OOA) is higher in summer (69%) than in winter (44%). Secondary aerosols

29   (sulfate+nitrate+ammonium+OOA) accounted for ~76% and 89% of NR-PM$_1$ mass in winter

30   and summer, respectively, indicating NR-PM$_1$ mass was driven mostly by secondary aerosol

31   formation regardless of the season. The mass loadings and diurnal patterns of these secondary

32   aerosols show a clear winter/summer contrast. Organic nitrate (ON) concentrations were

33   estimated using the NO$_x^+$ ratio method, with an average contribution of ~15% and 37% to OA

34   during winter and summer campaign, respectively. The estimated ON in summer strongly

35   correlated with LO-OOA ($r = 0.73$) and was enhanced at nighttime.

36   The relative importance of aqueous-phase chemistry and photochemistry in processing

37   OOA was investigated by examining the relationship of aerosol liquid water content (LWC)

38   and the sum of ozone (O$_3$) and nitrogen dioxide (NO$_2$) (O$_x$=O$_3$+NO$_2$) with LO-OOA and

39   MO-OOA. The processing mechanism of LO-OOA apparently depended on relative humidity

40   (RH). In periods of RH <80%, aqueous-phase chemistry likely played an important role in the

41   formation of wintertime LO-OOA, whereas photochemistry promoted the formation of

42   summertime LO-OOA. For periods of high RH >80%, these effects were opposite that of low

43   RH periods. Both photochemistry and aqueous-phase processing appear to facilitate MO-OOA

44   formation except during periods of high LWC, which is likely a result of wet removal during

45   periods of light rain.

46   The nighttime increases of MO-OOA during winter and summer were 0.013 and 0.01 μg

47   MO-OOA per μg of LWC, respectively. The increase of LO-OOA was larger than that for

48   MO-OOA, with increase rates of 0.033 and 0.055 μg LO-OOA per μg of LWC at night during

49   winter and summer, respectively. On average, the mass concentration of LO-OOA in summer

50   was elevated by nearly 1.2 μg m^{-3} for a ~20 μg change in LWC, which is accompanied by a 40

51   ppb change in O_x.

52

53   **1 Introduction**

54   Tropospheric particulate matter (PM) has adverse effects on air quality, visibility, and

55   ecosystems and participates in climate forcing (Watson, 2002; Grantz et al., 2003; Racherla and

56   Adams, 2006; Tai et al., 2010; Liu et al., 2017). The various effects of PM depend on its

57   physical, chemical and optical properties, which are determined by its emission, formation and

58   evolution/aging processes. Atmospheric PM can either be directly emitted from primary

59   sources (fossil fuel combustion, soil dust, sea salt, biomass burning, etc.) or formed through

60   chemical reactions of gaseous precursors, as is the case for secondary inorganic sulfate (SO_4^{2-})

61   and nitrate (NO_3^-) and secondary organic aerosol (SOA). Understanding the source

Atmospheric
Chemistry
and Physics
Discussions

Open Access

62   contributions and formation pathways of PM is essential for mitigating its effects (Jimenez et

63   al., 2009).

64   Houston, TX, is of great interest to the scientific community with respect to air quality, as

65   it is the fourth most populous city in the United States (U.S.) and is well known for its energy

66   and chemical industries. The annual average National Ambient Air Quality Standard (NAAQS)

67   for $PM_{2.5}$ (PM with diameter smaller than 2.5 micron) set by the U.S. Environmental Protection

68   Agency (EPA) was recently tightened from 15 to 12 $\mu g\ m^{-3}$ (US EPA, 2013), causing Houston

69   to be near non-attainment of this new standard, and creating a challenging for future NAAQS

70   attainment (Bean et al., 2016).

71   Numerous efforts, from modelling (McKeen et al., 2009; Li et al., 2015; Ying et al., 2015)

72   to field measurements (for example, TexAQS 2000 and II (Bates et al., 2008; Parrish et al.,

73   2009; Atkinson et al., 2010), Go-MACCS (McKeen et al., 2009; Parrish et al., 2009),

74   TRAMP2006 (Mao et al., 2010; Cleveland et al., 2012), GC-ARCH (Allen and Fraser, 2006),

75   SHARP (Olaguer et al., 2014), and DISCOVER-AQ (Bean et al., 2016; Leong et al., 2017))

76   have been made in the Houston metropolitan area during the past two decades, providing

77   critical insights into our understanding of air quality and atmospheric chemistry with respect to

78   the sources and formation of PM. Previous field campaigns underscore that OA accounts for a

79   major fraction of non-refractory submicron PM ($NR-PM_1$) in Houston (Bates et al., 2008;

80   Russell et al., 2009; Cleveland et al., 2012; Brown et al., 2013; Bean et al., 2016; Leong et al.,

81   2017; Wallace et al., 2018). The spatial variation of $NR-PM_1$ in Houston was investigated by

82   Leong et al. (2017), who divided the greater Houston into two zones based on marked

83   differences in $NR-PM_1$ levels, characteristics, and dynamics measured at 16 sampling locations.

Atmospheric
Chemistry
and Physics
Discussions

Open Access

EGU

84   Zone 1 is northwest of Houston and is dominated by SOA likely driven by nighttime biogenic

85   organic nitrate (ON) formation. Intensive attention has been paid recently to such

86   anthropogenic-biogenic interactions (Bahreini et al., 2009; Bean et al., 2016). Zone 2 is the

87   industrial/urban area south/east of Houston. Wallace et al. (2018) found mobile source exhaust

88   and petrochemical emissions likely are the most important factors impacting the NR-PM$_1$ and

89   trace gases at a site in Zone 2.

90   In terms of seasonal variation, many aerosol mass spectrometer (AMS) field campaigns

91   worldwide have been conducted in the summer (de Gouw et al., 2008; Takegawa et al., 2009;

92   Lefer et al., 2010; Crippa et al., 2013a; Hayes et al., 2013; Hu et al., 2016). Intense summertime

93   photochemical activity in Houston was observed during TRAMP 2006 relative to other field

94   studies (Mao et al., 2010), indicating the potential important role of photochemical oxidation in

95   SOA formation in the summer (Bahreini et al., 2009). In contrast, few measurements have

96   focused on wintertime aerosol (Crippa et al., 2013b; Chakraborty et al., 2015; Kim et al., 2017;

97   Wallace et al., 2008). Wintertime aerosol generally exhibits elevated mass loadings due to the

98   enhanced emissions from fuel combustion for heating and weather conditions favorable to

99   aerosol accumulation. Only a few studies present results based on long-term measurements for

100   seasonal comparison, such as in the SE U.S. (Xu et al., 2015; Budisulistiorini et al., 2016). The

101   knowledge gap regarding aerosol seasonal variability in Houston needs to be addressed to

102   improve regional air quality.

103   Formation of SOA in clouds and the aqueous phase of aerosol particles has been reported

104   worldwide (Lim et al., 2010; Ervens et al., 2011; Xu et al., 2017). Given that both

105   photochemical oxidation and aqueous-phase chemistry are conducive to the formation of SOA,

Atmospheric
Chemistry
and Physics
Discussions

106   it is of interest to compare the relative importance of photochemistry and aqueous-phase

107   chemistry for SOA formation in different seasons. The roles of photochemistry and

108   aqueous-phase processing on SOA formation and evolution in different seasons in Beijing have

109   been investigated by Hu et al. (2016) and Xu et al. (2017), respectively. Generally, the

110   aqueous-phase processing has a dominant influence on the formation of more oxidized SOA

111   and photochemical chemistry plays a major role in the formation of less oxidized SOA in

112   summer and winter in Beijing, while the relative importance of these two pathways in the

113   formation processes of SOA in autumn is different from those in summer and winter. The

114   relative roles of aqueous-phase and photochemical processes in the formation of SOA likely

115   vary with location and time. The seasonal differences in the spectral patterns, oxidation degrees

116   and contributions of SOA may result from different VOCs precursors, meteorological

117   conditions and atmospheric oxidizing capacity, which are not well understood in Houston,

118   particularly in different seasons.

119   This study presents observations of NR-PM$_1$ from two high-resolution time-of-flight AMS

120   (HR-ToF-AMS) measurement campaigns conducted during the winter and summer of 2014 at a

121   site in the suburbs of Houston, where industrial and vehicular emission sources and

122   photochemical processes are likely to play an important role in NR-PM$_1$ formation (Leong et

123   al., 2017). In addition to local emissions, this site was possibly impacted by regional marine

124   aerosol transported from the Gulf of Mexico (Schulze et al., 2018). The aims of this work are to

125   (1) investigate the seasonal characteristics of NR-PM$_1$ in the Houston area, (2) characterize the

126   primary and secondary sources by applying positive matrix factorization (PMF) analysis to the

127   measured OA mass spectra, and (3) evaluate the seasonal dependence of SOA composition and

Atmospheric
Chemistry
and Physics
Discussions

Open Access

EGU

128   formation, with a main focus on the relative effects of photochemistry and aqueous-phase

129   chemistry.

130

131   **2 Materials and Methods**

132   **2.1 Sampling Site and Campaigns**

133   Instrumentation was deployed in the University of Houston/Rice University Mobile Air

134   Quality Laboratory (MAQL), as described in Leong et al. (2017) and Wallace et al. (2018). The

135   winter campaign was conducted from February 3 through February 17, 2014, and the summer

136   campaign was conducted from May 1 to May 31, 2014. The measurement site was located on

137   the campus of University of Houston Sugar Land (UHSL) (29.5740 $^\circ$N, 95.6518 $^\circ$W). The

138   campus is situated southwest of downtown and the Houston Ship Channel (HSC). The map of

139   the measurement site is presented in Fig. S1 in the Supplemental Information (SI). The nearby

140   interstate highway (I-69) extends to the west of downtown and serves as a major traffic

141   emission source. The W.A. Parish Generating Station, a coal-fired power plant that is the

142   largest electricity generating facility in Texas, is ~6 miles south of the site (Fig. S1).

143   **2.2 Measurements**

144   The data used in this paper are reported in local time, which is 6 and 5 hours behind

145   Universal Coordinated Time (UTC) in winter and summer, respectively. The details regarding

146   the instrumental setup and data processing of these measurements were the same as described

147   in Wallace et al. (2018). The NR-PM$_1$ composition was measured using an Aerodyne

148   HR-ToF-AMS (DeCarlo et al., 2006; Canagaratna et al., 2007). A PM$_{2.5}$ Teflon®-coated

Atmospheric
Chemistry
and Physics
Discussions

149 cyclone inlet was installed above the MAQL trailer at a height of 6 m above ground to remove

150 coarse particles and to introduce air into the sampling line at a rate of 16.7 SLPM. A Nafion

151 dryer (Perma Pure, LLC) was mounted upstream of the HR-ToF-AMS to dry the sample to

152 below 45% relative humidity (RH). Particles are focused into a narrow beam via an

153 aerodynamic lens and accelerated under high vacuum into the particle sizing measurement

154 chamber. After passing the particle sizing chamber, the non-refractory components are flash

155 vaporized at near 600°C and ionized using electron impact at 70 eV. Ionized mass fragments are

156 then transmitted directly into the time-of-flight region so that the mass spectra can be obtained.

157 In this study, the HR-ToF-AMS was operated in "V-mode" to obtain the non-refractory

158 chemical components with a higher sensitivity, lower mass spectral resolution compared to the

159 "W-mode." Ionization efficiency (IE) calibration was performed monodisperse ammonium

160 nitrate (NH_4NO_3) at the beginning and end of each campaign. Filtered ambient air was sampled

161 every two days for approximately 20 to 30 min to provide a baseline of signal for the

162 HR-ToF-AMS during campaigns. The detection limits, (Table S1 in the SI) were calculated by

163 multiplying the standard deviations of the filter periods by three.

164   Trace gas mixing ratios and meteorological parameters also were measured on the MAQL

165 during the campaigns. Carbon monoxide (CO) was measured with high-resolution cavity

166 enhanced direct-absorption spectroscopy (Los Gatos Research, Inc.), and sulfur dioxide (SO_2)

167 was quantified using a pulsed fluorescence analyzer (ThermoFischer Scientific, model

168 43i-TLE). Nitric oxide (NO) and nitrogen dioxide (NO_2) were measured with a

169 chemiluminescence monitor with a UV-LED NO_2 photolytic converter on the NO_2 channel

170 (AQD, Inc.) The total reactive nitrogen (NO_y) was measured with a Thermo 49c-TL with a

8

171　heated Mo inlet converter. Ozone (O_3) mixing ratio was measured with ultraviolet absorption

172　(2BTech, Inc., model 205). Meteorological parameters including ambient temperature, solar

173　radiation, RH, wind speed (WS), and wind direction were measured using an RM Young

174　meteorological station.

175　**2.3 Data Processing**

176　The HR-ToF-AMS data analysis was performed using SQUIRREL v.1.56A and PIKA

177　v.1.16 in Igor Pro 6.37 (Wave Metrics Inc.). The relative ionization efficiencies (RIE) were

178　applied to OA (1.4), SO_4^{2-} (1.2), NO_3^- (1.1), NH_4^+ (4.0), and chloride (Cl^-, 1.3) following the

179　standard data analysis procedures. The composition-dependent collection efficiency (CE) was

180　applied to the data based on Middlebrook et al. (2012). Elemental ratios (H/C, O/C, N/C, and

181　S/C, where H is hydrogen, C is carbon, N is nitrogen, and S is sulfur) and the ratio of organic

182　mass to organic carbon (OM/OC) were generated using the procedures described by

183　Canagaratna et al. (2015).

184　**2.3.1 Quantification of the contributions of ON and Methanesulfonic Acid (MSA)**

185　*Estimation of ON.* The mass loading of NO_3^- measured by HR-ToF-AMS includes both

186　organic and inorganic NO_3^-. The fragmentation ratio of NO_2^+ to NO^+ (NO_x^+ ratio) is different

187　for ON and inorganic NO_3^- (Farmer et al., 2010; Fry et al., 2013), and the NO_2^+ and NO^+ mass

188　loadings for ON ($NO_{2,ON}$ and NO_{ON}) can be estimated using the method proposed by Farmer et

189　al. (2010):

190　$NO_{2,ON} = \frac{NO_{2,obs} \times (R_{obs} - R_{NO_3NH_4})}{R_{ON} - R_{NO_3NH_4}}$　　　　　(1)

191　$NO_{ON} = NO_{2,ON}/R_{ON}$　　　　　(2)

Atmospheric
Chemistry
and Physics
Discussions

Open Access

192   where R_{obs} is the ambient NO_x^+ ratio (0.531, 0.260 for the winter and summer campaign,

193   respectively, see Fig. S2 for details). $R_{NO_3NH_4}$(NO_x^+ ratio of NH_4NO_3) is determined by IE

194   calibration using monodisperse NH_4NO_3 before and after the campaigns. The average of the

195   two IE calibrations was used as the $R_{NO_3NH_4}$ for the campaign (0.588, 0.381 for the winter and

196   summer campaigns, respectively), which is comparable with the value reported elsewhere (Xu

197   et al., 2015; Zhu et al., 2016). The value of R_{ON} is hard to determine because it varies with

198   instruments and precursor volatile organic compounds (VOCs) (Fry et al., 2013). As

199   summarized by Xu et al. (2015), R_{ON} values ranging from 0.1 to 2.0 likely correspond to the

200   upper and lower bounds of the ON concentration estimated by the NO_x^+ ratio method. In this

201   work, R_{ON} is adopted as 0.166 as reported in literature (Fry et al., 2009). In winter, R_{obs} was

202   significantly higher than R_{ON} and close to $R_{NO_3NH_4}$, implying significant existence of

203   inorganic NO_3^-. In summer, R_{obs} was lower than $R_{NO_3NH_4}$ and close to R_{ON}, indicating a

204   significant fraction of the total NO_3^- is ON (Fig. S2).

205   The measured NO_x^+ ratio can be used to separately quantify ammonium and organic

206   nitrates as:

207    $$ON_{frac} = \frac{(R_{obs}-R_{NO3NH4})(1+R_{ON})}{(R_{ON}-R_{NO3NH4})(1+R_{obs})}$$ (3)

208   The nitrate functionality from organic nitrate was calculated as:

209    $$NO_{3,ON} = ON_{frac} \times NO_3^-$$ (4)

210   Thus, the nitrate functionality from inorganic nitrate (assuming NH_4NO_3 is the solely important

211   inorganic nitrate in the submicron mode) can be calculated as:

212    $$NO_{3,AN} = \left(1 - ON_{frac}\right) \times NO_3^-$$ (5)

Atmospheric
Chemistry
and Physics
Discussions

213   The estimation of the total mass of ON via this method is uncertain as the actual molecular

214   weight of the particle-phase species is unclear. Generally, the mass of ON is estimated by

215   assuming that the average molecular weights of organic molecules with nitrate functional

216   groups (value determined as described above) are 200 to 300 g mol^{-1} (Surratt et al., 2008;

217   Rollins et al., 2012). Previous work found that the nitrate radical (denoted as NO$_3$˙ with a dot to

218   differentiate it from aerosol NO$_3^-$) reaction with monoterpenes resulted in significant SOA

219   formation and that a hydroperoxy nitrate (C$_{10}$H$_{17}$NO$_5$) was likely a major NO$_3$˙-oxidized

220   terpene product in the southeastern U.S. (Ayres et al., 2015). Here, we use the molecular

221   weight of C$_{10}$H$_{17}$NO$_5$ (231 g mol^{-1}) to calculate the ON mass. Example periods of significant

222   ON contribution to PM are given in Fig. S3.

223   *Estimation of MSA.* During the two campaigns, there is no significant organic sulfur

224   contribution from other ion fragments except for CH$_3$SO$_2^+$. The concentration of MSA was

225   estimated as:

226     $$C_{MSA} = \frac{C_{CH3SO2}}{f_{MSA,CH3SO2}}$$ (6)

227   where C_{CH3SO2} is the concentration of ion fragment CH$_3$SO$_2^+$ (*m/z*=78.99) and the fraction of

228   CH$_3$SO$_2^+$ to the total signal intensity of all the fragments of pure MSA, $f_{MSA,CH3SO2}$, is 5.55%.

229   This values was observed for the mass spectra of pure MSA in laboratory experiments (Schulze

230   et al., 2018) and is comparable to previous work (Huang et al., 2015).

231   **2.3.2 Positive Matrix Factorization (PMF) Analysis**

232   The PMF technique has been used widely for source apportionment (Paatero and Tapper,

233   1994), including with HR-TOF-AMS data (Ulbrich et al., 2009; Zhang et al., 2011). The

234   high-resolution NR-PM$_1$ OA mass spectra matrix (m/z =12 to m/z=130) and the associated

235   error matrix obtained by using PIKA v 1.19 D were used for PMF analysis. Data were prepared

236   according to the protocol proposed by Ulbrich et al. (2009) and Zhang et al. (2011) prior to

237   PMF analysis. The PMF model was used to decompose the measured OA mass spectra matrix

238   by solving:

239     $\text{X} = \text{GF} + E = \sum_{p=1}^{J} G_{ip}F_{pj} + E_{ij}$ (7)

240   where X is the $m \times n$ matrix of measurement data, the m rows of X are the OA mass spectra

241   measured at each time step, the n columns of X are the time series of each organic

242   mass-to-charge ratio, and p is the number of factors. G_{ip} is the matrix that denotes the

243   contributions of factor p at time step i, and F_{pj} represents the factor mass spectral profiles. E

244   is the residual matrix. The least-squares algorithm is used to fit the data to minimize iteratively

245   a quality of fit parameter, Q:

246     $\text{Q} = \sum_I \sum_J (E_{ij}/\sigma_{ij})^2$ (8)

247   where σ_{ij} is the matrix of estimated errors of the data.

248   Solutions using PMF with 2 to 7 factors were explored. The best solution with the

249   optimum number of factors was evaluated carefully using an open source PMF evaluation tool

250   (PET v 2.08D, (Ulbrich et al., 2009)) following the procedures described in Zhang et al. (2011).

251   Selection criteria included 1.) variation of the ratio of Q to expected Q$_{exp}$ (*mn−p(m+n)*, the

252   degrees of freedom of the fitted data (Paatero et al., 2002)) after adding an additional factor, 2.)

253   agreement between the reconstructed OA mass concentrations and the measured concentrations,

254   3.) scaled residuals for the different ion fragments included in the dataset and variations of the

Atmospheric
Chemistry
and Physics
Discussions

255   residual of the solution as a function of time, 4.) agreement between factor time series and time

256   series of external tracers/individual ions, and 5.) examination of factor profiles. The last two are

257   considered to determine the physical meaningfulness of the factors. The PMF solution with

258   factor numbers greater than five and four for winter and summer dataset, respectively, yielded

259   no new distinct and physical meaningful factors. The Q/Q_{exp} and the factors obtained for

260   different FPEAK (from -1 to 1 with a step value of 0.2) values resulted in a small difference in

261   the OA components. Because of the lowest Q/Q_{exp} and because the use of FPEAK values

262   different from 0 did not improve the correlations between PMF factors and potentially

263   associated tracers, the five- and four-factors solutions with FPEAK=0 can be well interpreted in

264   winter and summer, respectively. The convergence of the PMF model containing five- and

265   four-factors were examined by running each model from fifteen different starting values

266   (SEEDs 0-30 with a step value of 2). The small variation observed in Q/Q_{exp} and the mass

267   fraction of different factors as SEED changed indicates the solutions were stable. As a result,

268   SEED 0 was chosen for the final solution. The factors were interpreted as hydrocarbon-like OA

269   (HOA), biomass burning OA (BBOA), cooking OA (COA, identified only in the winter

270   campaign), and two oxidized OA (named less-oxygenated (LO-) OOA and more-oxygenated

271   (MO-) OOA). The data treatment, factor selection and interpretation are detailed in the SI.

272   **2.3.3 Estimation of Aerosol Liquid Water Content (LWC)**

273   Aerosol LWC includes water associated with organic aerosol and inorganic aerosol, which

274   were calculated using an empirical method and a thermodynamic model, respectively.

275   Inorganic LWC (W_i) was predicted by ISORROPIA-II in forward mode in mol L^{-1} (Fountoukis

276   and Nenes, 2007). Inputs for ISORROPIA-II include inorganic aerosol mass concentrations

277 (SO_4^{2-}, inorganic NO_3^-, and ammonium (NH_4^+)) and meteorological parameters (temperature

278 and RH). Calculation empirical of organic LWC (W_O) follows (Petters and Kreidenweis, 2007;

279 Guo et al., 2015):

280 $W_O = \frac{m_{org}\rho_w}{\rho_{org}} \frac{\kappa_{org}}{(1/RH - 1)}$ (9)

281 where m_{org} is the organic mass concentration (μg m^{-3}), and ρ_w is the density of water (1 g

282 cm^{-3}). The organic density (ρ_{org}, g cm^{-3}) was estimated using an empirical equation based on

283 elemental ratios (Kuwata et al., 2012; Guo et al., 2015):

284 $\rho_{org} = 1000 \times [\frac{12 + \frac{H}{C} + 16 \times \frac{O}{C}}{7.0 + 5 \times \frac{H}{C} + 4.15 \times \frac{O}{C}}]$ (10)

285 The hygroscopicity of SOA generated during chamber studies under sub-saturated regimes

286 depends on the OA degree of oxidation (Prenni et al., 2007; Jimenez et al., 2009; Petters et al.,

287 2009; Chang et al., 2010). A simple linear relationship between the OA degree of oxidation

288 (defined as the fraction of the total signal at m/z 44, f$_{44}$) and hygroscopicity (κ_{org}) is used

289 (Duplissy et al., 2011):

290 $\kappa_{org} = 2.2 \times f_{44} - 0.13$ (11)

291 The total LWC is then found by summing the water content associated with each mass fraction:

292 $LWC = W_i + W_O$ (12)

293

294 **3 Results and Discussion**

295 **3.1 Temporal Dependences of Submicron Aerosol Composition**

296 Campaign overview data for winter and summer are shown in Fig. 1, including

297   meteorological parameters (e.g., temperature, RH, radiometer, wind direction and speed), trace

298   gases (e.g., CO, SO_2, NO, NO_2, and O_3), chemically resolved NR-PM_1 concentrations, OM/OC,

299   and elemental ratios (H/C, O/C, N/C and S/C). Data also are shown in Table 1.

300   Data indicate that the average concentration of NR-PM_1 during winter campaign was $6.0 \pm$

301   3.7 µg m^{-3}, ranging from 0.5 to 14.8 µg m^{-3}. Mass loadings of NR-PM_1 at this measurement site

302   are relatively smaller than a site near the HSC in winter 2015 (10.8 µg m^{-3} (Wallace et al.,

303   2018)), perhaps suggesting a weaker industrial influence at the UHSL site.

304   The average concentration of NR-PM_1 during summer was 3.6 ± 1.7 µg m^{-3}, ranging from

305   0.3 to 13.7 µg m^{-3}. For comparison, a summer campaign in 2006 on an elevated building near

306   downtown Houston showed an average NR-PM_1 concentration of approximately 11 µg m^{-3}

307   (Cleveland et al., 2012). An elevated NR-PM_1 episode was observed from May 28-31 (Fig.

308   1(m)), with high solar radiation and O_x ($O_x = NO_2 + O_3$) levels during the daytime, and high

309   RH at night, resulting in OA becoming the largest fractional species, likely due to gas-phase

310   photochemical production of SOA together with the nighttime increase of SOA associated with

311   high RH, lowered boundary layer and cooler temperatures.

312   In winter, OA was the largest component of NR-PM_1, accounting for $45.5 \pm 13.3\%$ on

313   average of the total mass, followed by SO_4^{2-} ($19.9 \pm 11.2\%$), $NO_3^-{}_{,AN}$ ($17.2 \pm 10.8\%$), NH_4^+

314   ($13.2 \pm 5.4\%$), $NO_{3,\ ON}$ ($3.4 \pm 1.4\%$) and Cl^- ($0.9 \pm 0.2\%$) (Fig. 2). Primary OA

315   (POA=HOA+BBOA+COA) was responsible for $59.1 \pm 19.2\%$ of OA mass. Secondary species

316   ($SO_4^{2-}+NO_3^-+NH_4^++$LO-OOA+MO-OOA) accounted for $\sim72.3 \pm 18.1\%$ of NR-PM_1 mass,

317   which is higher than that in winter in Seoul (Kim et al., 2017) and Beijing (Hu et al., 2016).

318   The inorganic aerosols in the winter were mostly neutralized in the forms of NH_4^+ salts (e.g.,

319    $(NH_4)_2SO_4$, NH_4NO_3, NH_4Cl) based on the predicted-to-measured NH_4^+ ratio of ~1 with

320   correlation coefficient (r^2) of 0.98 (Fig. 3(A)).

321   In contrast to winter, OA during the summer campaign constituted on average $54.6 \pm 18.2\%$

322   of NR-PM$_1$ mass, and SO_4^{2-} was the second largest component ($30.9 \pm 15.5\%$), followed by

323   NH_4^+ ($12.2 \pm 5.2\%$). $NO_{3,ON}^-$ and $NO_{3, AN}$ only accounted for $1.5 \pm 1.9\%$ and $0.4 \pm 0.8\%$ of

324   NR-PM$_1$ mass in the summer, respectively. Cl^- contributed $0.4 \pm 0.5\%$ of NR-PM$_1$ mass. The

325   increased PBL height in summer (Haman et al., 2012) likely contributed to relatively lower

326   trace gas and NR-PM$_1$ levels in the summer. Secondary species contributed $\sim87.3 \pm 14.2\%$ of

327   NR-PM$_1$ mass, indicating that the relative importance of secondary aerosol formation increased

328   during summer as compared to winter, especially for species such as SO_4^{2-} and MO-OOA.

329   The total OA displayed high values during the nighttime hours in both winter and summer,

330   maintaining a high level until morning rush hour, and then decreasing to a minimum value after

331   9:00 (Fig. 4). The summertime OA presented a small peak at noon, suggesting that

332   photochemical formation of OA played a more important role in summer than in winter.

333   Increasing of ambient temperature and PBL height after sunrise causes re-partitioning to the gas

334   phase, likely contributing to the decrease of OA, LO-OOA and ON during daytime.

335   Contributions of PMF factors to wintertime and summertime OA show significant

336   differences. For wintertime OA, on average, BBOA, MO-OOA, and COA made similar

337   contributions of 24%, 23% and 22% to total OA mass, respectively. The LO-OOA accounted

338   for 18% of OA mass, followed by HOA (13%). The POA constituted more than half of OA

339   mass (59%), with the remainder of being OOA (41%). In the summer, LO-OOA represented the

340   largest fraction of the OA mass (53% on average), followed by MO-OOA (24%), HOA (12%)

Atmospheric
Chemistry
and Physics
Discussions

341   and BBOA (11%). In the case of summer, OOA constituted 77% of OA and 42% of total

342   NR-PM$_1$ mass, which are almost two times their relative contributions in winter. The time

343   series of mass concentrations of NR-PM$_1$ species (Fig. 1) and OA factors (Fig. 5) in summer

344   were relatively stable and repeatable, while it changed dramatically in winter due to the

345   different meteorological conditions.

346   **3.2 Seasonal Variation of the Formation of Sulfate and Nitrate**

347   During the summer campaign, the prevailing southerly winds from the Gulf of Mexico

348   carry marine aerosols to Houston (Schulze et al., 2018), resulting in a relatively high fraction of

349   SO_4^{2-} and MSA. As shown in Fig. 1(m, j), the increased contribution of SO_4^{2-} occurred when

350   winds originated from the south at a high speed (e.g., May 16-27), while the contribution of

351   SO_4^{2-} decreased significantly when winds originated from the north (e.g., May 10th and May

352   13-15). MSA and S/C were markedly elevated during periods of southerly winds (Fig. 1(o, p)),

353   and O/C and OM/OC were relatively higher (Fig. 1(n)). In addition, elevated SO$_2$ plumes were

354   recorded during periods of southerly winds (Fig. 1(j, k)), potentially as a result of emissions

355   from the Parish coal-fired power plant. In contrast to SO_4^{2-}, the fractional contribution of NO$_3$

356   and OA increased greatly when the winds were not southerly. Primary pollutants such as CO,

357   NO and NO$_2$, were elevated when winds were northerly (Fig. 1(k)), accompanied by lower O/C

358   and higher H/C ratios during the corresponding periods (Fig. 1(n), e.g., May 1st, 2rd, 10th, 15th).

359   Diurnal patterns of NR-PM$_1$ and other species in the winter and summer (Fig. 4) suggest

360   significant seasonal dependence of sources and formation processes of NR-PM$_1$ species in

361   Houston. In the case of SO_4^{2-}, the diurnal pattern displayed a daytime peak in both winter and

362   summer, with the peak much more pronounced in summer mid-day. In winter, the f_{SO4} (mole

Atmospheric
Chemistry
and Physics
Discussions

363   ratio of [SO_4^{2-}] to the sum of [SO_2] and [SO_4^{2-}]) and LWC have concurrent peak value during

364   the night time. However, there is no obvious correlation between f_{SO4} and LWC in summer,

365   though a moderate correlation ($r = 0.44$) was found in winter (Fig. 3). These results suggest that

366   SO_4^{2-} formed though aqueous-phase chemistry in winter is more prominent than that in

367   summer.

368   The total nitrate concentration was higher in winter than in summer. $NO_3^-{}_{,AN}$ was very low

369   in summer due to its thermal instability under high temperature, while it was relatively

370   enhanced in winter. According to the NO_x^+ ratio method described in Sec. 2.3.1, the mass

371   fraction of $NO_3^-{}_{,AN}$ in total nitrate was decreased from 90% (1.26 µg m^{-3}) in winter to 48%

372   (0.04 µg m^{-3}) in summer. The concentration of $NO_{3,ON}$ was 0.14 µg m^{-3} in winter, which is 3.5

373   times that in summer. The seasonal variation of $NO_3^-{}_{,AN}$ is much stronger than that of $NO_{3,ON}$.

374   This is in accordance with previous observations in Atlanta, Georgia and Centreville, Alabama

375   (Xu et al., 2015).

376   The diurnal profiles of $NO_{3,ON}$ show that it reached peak value before dawn in both seasons

377   (Fig. 6). However, $NO_3^-{}_{,AN}$ presents a bimodal diurnal profile in both seasons. The $NO_3^-{}_{,AN}$,

378   which increased from late afternoon and peaked at 2:00-4:00, was likely formed through

379   nighttime chemistry from dinitrogen pentoxide (N_2O_5) hydrolysis, as the LWC displayed a

380   trend similar to that of $NO_3^-{}_{,AN}$, This was corroborated by the observation of O_x (>25 ppb),

381   which is needed to form N_2O_5 (via $NO_3^{\cdot}$). The second peak observed during morning rush hour

382   was likely formed though photochemical processing of NO_x emitted from vehicles because the

383   traffic flow and O_x level are elevated during morning rush hour. The decreasing trend of

384   $NO_3^-{}_{,AN}$ after 9:00 is presumed to be a result of enhanced PBL height and evaporation.

Atmospheric
Chemistry
and Physics
Discussions

385   The estimated ON accounted for ~1 to 57% of the total NR-PM$_1$ and 1 to 99% percent of

386   the OA with an average contribution of about 12 and 37% to both, comparable to other studies

387   (Fry et al., 2009; Rollins et al., 2010; Xu et al., 2015; Berkemeier et al., 2016). In winter, ON,

388   on average accounted for 35 and 15% of NR-PM$_1$ and OA mass, respectively. Figure S3

389   presents a high ON loading period observed in summer.

390   A proxy for NO$_3^{\cdot}$ production rate is based on the product of the observations of [NO$_2$] and

391   [O$_3$] (Rollins et al., 2012), where brackets represent mixing ratios in ppb. The O$_x$ (> 25 ppb)

392   and elevated NO$_x$ observed at night in summer (Fig. 4) resulted in rapid NO$_3^{\cdot}$ formation. Thus,

393   the concurrent enhancement in ON and O$_3$ times NO$_2$ occurring during nighttime (Fig. S3)

394   presumably was caused by the nocturnal NO$_3^{\cdot}$-initiated oxidation of anthropogenic and

395   biogenic VOCs, with the latter probably larger than the former (Brown et al., 2013). The high

396   N/C ratio of LO-OOA, concurrent peak value in LO-OOA and ON during nighttime hours (Fig.

397   4), and appreciable correlation of LO-OOA and ON in summer (r = 0.73) (Fig. 5) together

398   suggest that particle-phase ON from NO$_3^{\cdot}$-initiated chemistry contributed to nighttime

399   LO-OOA in summer.

400

401   **3.3 Effects of Aqueous-phase and Photochemical Oxidation on OOA Formation**

402   On average, OOA accounted for 41 ± 19% of OA mass in winter but increased to 77 ± 16%

403   in summer. Note that MO-OOA accounted for more than half of OOA in winter (56%),

404   indicating the more important role of MO-OOA in winter as compared to LO-OOA on a

405   relative basis. In contrast, LO-OOA dominated OOA in summer (69%). The mass spectra of

406   MO-OOA in winter and summer are similar (Fig. 7, r = 0.84) as are the extent of oxidation

Atmospheric
Chemistry
and Physics
Discussions

407   (O/C = 1.10 versus 1.07). However, LO-OOA in winter showed a different spectral pattern

408   compared with that in summer. The mass spectrum of LO-OOA in winter was characterized by

409   high m/z 32 (mainly CH_4O^+) and 46 (mainly $CH_2O_2^+$) peaks, resulting in a relatively high O/C

410   (0.89) in winter that suggest LO-OOA in winter was more aged than that in summer

411   (O/C=0.74).

412   Sun et al. (2016) reported a unique OOA in ambient air, termed aq-OOA

413   (aqueous-phase-processed SOA), that strongly correlated with particle LWC, sulfate and

414   S-containing ions. As shown in Table 2, by comparing the mass spectra of OOA in this work

415   with aq-OOA, it is found that the mass spectra of MO-OOA in winter in this study presents a

416   much stronger correlation (r =0.96) with aq-OOA, rather than LO-OOA in winter in this study

417   (r =0.75). Both MO-OOA and LO-OOA in summer highly correlated with aq-OOA. This result

418   indicates that the formation of LO-OOA in summer and MO-OOA in both seasons may involve

419   aqueous-phase chemistry.

420   Assuming that OOA deduced from PMF analysis can be used as a surrogate of SOA (Wood

421   et al., 2010; Xu et al., 2017), the two OOA were used to investigate the formation mechanisms

422   and evolutionary processes of SOA. Previous studies have found SOA correlated well with odd

423   oxygen (O_x) in many cities (Wood et al., 2010; Sun et al., 2011; Hayes et al., 2013; Zhang et al.,

424   2015; Xu et al., 2017) and that SOA formation is significantly impacted by aqueous-phase

425   processing (Lim et al., 2010; Ervens et al., 2011; Xu et al., 2017). The relationships between

426   OOA factors and O_x/LWC were used as the metrics to characterize SOA formation mechanisms

427   associated with photochemistry/aqueous oxidation chemistry (Xu et al., 2017).

428   Fig. 8 (A, B) indicates the LWC frequency distribution. Winter LWC are binned in 5 μg

20

Atmospheric
Chemistry
and Physics
Discussions

429   m^{-3} increments from 0 to 20 $\mu g\ m^{-3}$. Data in the ranges of 20 to 30 $\mu g\ m^{-3}$, 30 to 50 $\mu g\ m^{-3}$, 50

430   to 80 $\mu g\ m^{-3}$, and 80 to 120 $\mu g\ m^{-3}$ are shown as 25, 40, 65 and 100 $\mu g\ m^{-3}$, respectively.

431   Summer LWC are binned in 2.5 $\mu g\ m^{-3}$ increments from 0 to 15 $\mu g\ m^{-3}$. The bins shown as 17.5

432   and 27.5 $\mu g\ m^{-3}$ represent data from 15 to 20 $\mu g\ m^{-3}$ and 20 to 35 $\mu g\ m^{-3}$.

433   The data associated with the artificially created bins in both seasons did not pass the

434   normal test and homogeneity test of variances. The statistical significance of differences

435   between bins was then tested using the Kruskal-Wallis analysis of variance (K-W ANOVA).

436   The differences between winter and summer data of the bins were significant. Thus, the

437   Dunn-Bonferroni test was performed for the *post-hoc* pairwise comparisons. It was found that

438   the difference of all measured variables in different bins shown in Fig. 8 were significant

439   ($p<0.01$). The results can be found in Tables S5-S6. Fig. 8(C, D) presents a clear positive trend

440   of RH as a function of LWC in both winter and summer which implies an increased potential

441   for aqueous-phase processing at high RH level, enhanced by low wind speed that allows

442   accumulation of pollutants (Fig. 8(E, F)). The patterns of other parameters as LWC increases in

443   winter were different from those in summer.

444   The variation of binned mean OA mass against LWC presents significant seasonal

445   difference (Fig. 8(A, B)). In winter, the OA mass increased when LWC increased from 2.5 to

446   12.5 $\mu g\ m^{-3}$ but decreased as the LWC increased further. The LO-OOA mass decreased

447   dramatically when LWC>12.5 $\mu g\ m^{-3}$ (RH>80%, Fig. 8(C)) while MO-OOA continues

448   increasing until LWC> 40 $\mu g\ m^{-3}$. This result indicates that wet removal may dominate under

449   an extremely high RH environment coupled with stagnant air (WS <2 m/s Fig. 8(E)). In

450   summer, the OA mass decreased when LWC increased from 1.25 to 6.25 $\mu g\ m^{-3}$ but increased

Atmospheric
Chemistry
and Physics
Discussions

451   when LWC increased further, suggesting the wet removal effect is not as strong as that in

452   winter because of the relatively lower LWC in summer than in winter.

453   On average, LO-OOA (Fig. 8(G, H)) in winter increased from 0.3 to 0.9 μg m^{-3} when LWC

454   increased from 2.5 to 7.5 μg m^{-3} but decreased as the LWC increased further, particularly when

455   LWC >40 μg m^{-3}. The slope of this decrease was approximately -0.008 μg LO-OOA μg^{-1} LWC.

456   Fig. 8(A) shows that 64% of the data points were observed in the situation of low LWC (<12.5

457   μg m^{-3}, RH<80%), when the increase of LO-OOA was more significant than that of MO-OOA.

458   In contrast, LO-OOA in summer showed a decreased trend under low LWC level (LWC<6.25

459   μg m^{-3}, RH<80%) but a significant linear increase from approximately 0.77 μm^{-3} to 1.8 μg m^{-3}

460   as LWC increased from 6.25 to 27.5 μg m^{-3}, a slope of 0.053 μg LO-OOA μg^{-1} LWC. The

461   relatively high LO-OOA under low LWC level was likely more regional, with contributions

462   from possibly transported non-aqueous OOA, as the wind speed in this case was relatively high

463   and RH was low. The formation of LO-OOA under high LWC level was likely enhanced by

464   local aqueous-phase heterogeneous chemistry.

465   MO-OOA (Fig. 8(I, J)) slightly increased during both seasons as LWC increased. In winter,

466   MO-OOA presented a similar linear increase trend from 0.57 to 0.98 μg m^{-3} when LWC

467   increased from 2.5 to 40 μg m^{-3} but decreased as the LWC increased further (probably due to

468   the wet removal effect). The slope of this increase was approximately 0.008 μg MO-OOA μg^{-1}

469   LWC. In summer, MO-OOA appears to increase from 0.49 to 0.64 μg m^{-3} when LWC increased

470   from 2.5 to 27.5 μg m^{-3}, with slope of 0.005 μg MO-OOA μg^{-1} LWC. In winter, because of the

471   decrease in LO-OOA with LWC, the relative fraction of MO-OOA increases as LWC increases.

472   The mutual effect of aqueous-phase and photochemistry on OOA formation prevents solely

Atmospheric
Chemistry
and Physics
Discussions

473   evaluating the role of the two processes. Sullivan et al. (2016) reported multiple lines of

474   evidence for local aq-SOA formation observed in the Po Valley, Italy during times of increasing

475   RH, which coincided with dark conditions. Thus, the daytime data were separated to examine

476   the variation of OOA against O_x. The relationship between OOA and aqueous-phase chemistry

477   was investigated further by excluding the daytime data, with the aim of diminishing the

478   influence of photochemistry. To do so, nighttime and daytime were based on sunrise and sunset

479   in Houston during the two campaigns (https://www.timeanddate.com/sun/usa/houston). On

480   average, the day lengths are 11 h 10 min and 13 h 35 min for the campaigns in February and

481   May, 2014, respectively.

482   Figure 9 presents the scatter plots of OOA versus LWC during nighttime for the two

483   campaigns. The green dots denote the increasing trend of OOA against LWC. It is found that

484   the increase of wintertime LO-OOA under low LWC level (<20 µg m^{-3}) during the night is

485   stronger than that shown in Fig. 8 (G). The nighttime LO-OOA linearly increased from 0.04 to

486   0.64 µg m^{-3} when LWC increased from 2.5 to 17.5 µg m^{-3}, a slope of 0.033 µg LO-OOA µg^{-1}

487   LWC. This result indicates that the nighttime increase in LO-OOA in winter is more likely

488   formed via aqueous-phase chemistry in aerosol liquid water. In contrast, the increase of

489   LO-OOA under high LWC level (LWC>6.25 µg m^{-3}) in summer was less enhanced during

490   nighttime (0.055 µg LO-OOA µg^{-1} LWC) as compared to the increase rate of whole dataset

491   (0.053 µg LO-OOA µg^{-1} LWC). The slope of nighttime increase of MO-OOA against LWC

492   during the winter campaign was 0.013 µg MO-OOA µg^{-1} LWC, which is 1.7 times the slope for

493   the whole dataset (daytime and nighttime). For the summer campaign, the increase of nighttime

494   MO-OOA is 2.2 times the rate for the whole dataset.

495   These results suggest that aqueous-phase processing likely has a strong positive impact on

496   the formation of MO-OOA in the two seasons except for instances when LWC exceeds 100 μg

497   m^{-3} in winter. It also appears to facilitate the local formation of LO-OOA under low LWC level

498   (<17.5 μg m^{-3}) in winter and under relatively high LWC level (>6.25 μg m^{-3}) in summer.

499   As mentioned previously, ON contributes significantly to summertime LO-OOA, and the

500   concurrent enhancement in ON and LO-OOA during night was associated with elevated RH

501   (Fig. 4). A previous study found that the partitioning of organic compounds to the particle phase

502   was significantly increased at elevated RH levels (70%) in an urban area dominated by

503   biogenic emissions in Atlanta (Hennigan et al., 2008). The correlation of ON and LO-OOA in

504   summer nighttime (r=0.76) was stronger than that during daytime (r =0.53). Thus, we presume

505   that aerosol water facilitates the formation of ON from NO$_3$˙-initiated chemistry involving

506   BVOCs during nighttime, resulting in a good relationship of LO-OOA and LWC in summer.

507   MSA is a secondary product from the oxidation of dimethyl sulfide (DMS) (Zorn et al.,

508   2008), which is a gaseous species emission from marine organisms (Barnes et al., 2006). Thus,

509   MSA is found to be abundant in marine/coastal areas and play an important role in the

510   formation of marine PM (Gondwe, et al., 2004; Huang et al., 2015; Schulze et al., 2018). The

511   formation of MSA is unique to aqueous-phase processing, and could be used as an indicator of

512   aqueous SOA formation (Barnes et al., 2006; Ervens et al., 2011). Recent observations

513   confirmed that MSA and associated fragment ions (CH$_2$O$_2^+$ (m/z 46), C$_2$O$_2^+$ (m/z 56) and

514   C$_2$H$_2$O$_2^+$ (m/z 58), which are unique ions of glyoxal and methylglyoxal uptake on SOA

515   (Chhabra et al., 2010)) strongly correlated with SOA formed via aqueous-phase processing (Ge

516   et al., 2012; Sun et al., 2016). In this work, the MO-OOA formation was associated with

Atmospheric
Chemistry
and Physics
Discussions

517   aqueous-phase oxidation more strongly than LO-OOA in winter, which likely can be further

518   verified by the correlations between MO-OOA/LO-OOA and MSA. As shown in Fig. 7, MSA

519   has a relatively higher correlation coefficient with MO-OOA (r=0.45) compared to LO-OOA

520   (r=0.30), though the correlation also is influenced by many other factors.

521   Fig. 10 (A, B) presents the frequency distribution of O_x. Winter O_x are binned in 10 ppb

522   increments from 0 to 60 ppb. The range for summer is 20 to 70 ppb. The data associated with

523   the artificially created O_x bins in both seasons did not pass the normal test and homogeneity test

524   of variances. The K-W ANOVA for winter and summer data of the bins were significant. The

525   Dunn-Bonferroni test for the *post-hoc* pairwise comparisons shows that the difference of

526   measured variables among different bins shown in Fig. 10 were significant (Tables S7-S8). The

527   clear positive relationship between solar radiation and O_x is shown in Fig. 10 (C, D), and the

528   negative relationship between solar radiation and RH is shown in Fig. 10 (E, F), suggesting

529   strong atmospheric photochemical activity associated with high O_x periods.

530   The variations of LO-OOA and MO-OOA showed substantially different patterns with

531   increases of O_x in winter and summer. In winter, LO-OOA and MO-OOA showed comparable

532   increasing trends at low O_x level (<35 ppb), with MO-OOA having a stronger response. The

533   LO-OOA was increased from 0.13 to 0.72 μg m^{-3} when O_x increased from 5 to 35 ppb but

534   decreased as the O_x increased further. The slope of this increase was approximately 0.023 μg

535   LO-OOA ppb^{-1} O_x. MO-OOA increased from 0.13 to 0.88 μg m^{-3} when the O_x increased from 5

536   to 35 ppb, with a slope of 0.027 μg MO-OOA ppb^{-1} O_x. This leads to a maximum in the mass

537   fraction of MO-OOA in the mid-O_x level range and also at highest levels of observed O_x.

538   In summer, there is a clear decreasing trend of RH with increases of O_x. As discussed

539   previously, the high level of summertime LO-OOA likely was associated with high LWC.

540   Therefore, the high mass fraction of LO-OOA at the lowest O_x level (<20 ppb) associated with

541   the high RH/LWC was likely from aqueous-phase chemistry. After excluding low O_x data (<20

542   ppb), LO-OOA showed a much stronger response to O_x than did MO-OOA. The summer

543   LO-OOA showed a significant linear increase from approximately 0.6 to 1.8 µg m^{-3} when O_x

544   increased from 25 to 65 ppb, a slope of 0.03 µg LO-OOA ppb^{-1} O_x. This increase was likely in

545   the case of low RH conditions (<80%, Fig. 8 (D)), when aqueous-phase chemistry did not

546   promote the formation of LO-OOA (Fig. 8 (H)). Summer MO-OOA increased from 0.36 to

547   0.67 µg m^{-3} when O_x increased from 25 to 55 ppb but decreased as the O_x increased further.

548   The slope of this increase was 0.007 µg MO-OOA ppb^{-1} O_x. Contrary to winter, LO-OOA

549   responded more strongly to increases of O_x than MO-OOA did.

550   The relationship of OOA versus O_x was examined further by excluding nighttime data.

551   Figure 11 presents the scatter plots of daytime OOA versus O_x for the winter and summer

552   campaign. The daytime responses of LO-OOA and MO-OOA to O_x in winter were ~1.5 times

553   that for the whole dataset (Fig. 10 (G, I)), and the increase rate of MO-OOA was higher than

554   that of LO-OOA. In summer, the slope of the daytime increase of LO-OOA was 1.24 times that

555   for the whole campaign (Fig. 10 (H)), and the increase rate of daytime MO-OOA was close to

556   that for whole dataset. These results suggest that the photochemical enhancement of OOA in

557   winter was more prominent than that in summer. For the summer campaign, the formation of

558   LO-OOA was more strongly linked to photochemistry compared to MO-OOA. At low

559   atmospheric oxidative capacity (Ox<20 ppb), aqueous-phase chemistry was likely predominant

560   in the formation of LO-OOA.

Atmospheric
Chemistry
and Physics
Discussions

561   The combined effects of photochemistry and aqueous-phase chemistry on OOA

562   composition during winter and summer are further demonstrated in Fig. 12. The ratio of

563   MO-OOA/LO-OOA in winter showed the highest values on the left-top corner in Fig. 12 (A),

564   suggesting photochemical processing was likely responsible for MO-OOA formation, under

565   low LWC levels (< 10 μg m^{-3}). Additionally, data with high MO-OOA/LO-OOA on the

566   right-bottom corner in Fig. 12 (A) indicate the important role of aqueous-phase chemistry under

567   low O_x and high LWC levels. Overall, the concentration of MO-OOA in winter increased as

568   O_x/LWC increased, whereas LO-OOA markedly decreased. This result indicates both

569   photochemical and aqueous-phase processing played a more important role in enhancing

570   MO-OOA than LO-OOA in winter. Furthermore, the diurnal patterns of wintertime LO-OOA

571   only presented a peak value at night while MO-OOA showed one peak value at night (high

572   LWC) and another one in the afternoon (high O_x period) (Fig. 4).

573   In summer, data points with low MO-OOA/LO-OOA value on the left-top of Figure 12 (B)

574   illustrated that LO-OOA was enhanced in high-O_x and low-LWC condition, though the low

575   MO-OOA/LO-OOA are not confined to just the top left. In case of high LWC level (LWC> 6.5

576   μg m^{-3}), MO-OOA/LO-OOA were much lower (on the right of Figure 12 (B), particularly when

577   LWC> 10 μg m^{-3}). Although MO-OOA increased with LWC and O_x, the increase of LO-OOA

578   was more significant. The effects of both photochemistry (≥ 25 ppb) and aqueous-phase

579   chemistry (≥ 6.5 μg m^{-3}) were more relevant for the formation of LO-OOA than MO-OOA. On

580   average, the mass concentration of LO-OOA was elevated by nearly 1.2 μg m^{-3} as a ~20 μg

581   change in LWC (increased from 6.25 μg m^{-3} to 27.5 μg m^{-3}, Fig. 8 (H)), which is equivalent to

582   a 40 ppb change in O_x (increased from 25 ppb to 65 ppb, Fig. 10 (H)). This result further

Atmospheric
Chemistry
and Physics
Discussions

583   suggests that the aqueous-phase chemistry is comparable to photochemistry in processing

584   LO-OOA in summer. The diurnal pattern of summertime LO-OOA displays a peak value at

585   night and a comparable peak value in the afternoon (Fig. 4).

586

587   **4 Conclusions**

588   Seasonal characterization of NR-PM$_1$ collected using HR-ToF-AMS near Houston in 2014

589   demonstrated that the mass loading, diurnal patterns, and important formation pathways of

590   NR-PM$_1$ vary seasonally. The OA was the largest component of NR-PM$_1$ mass, on average,

591   accounting for 46% and 55% of the mass loadings in winter and summer, respectively, which is

592   less than that in the north part of Houston, which is influenced by high biogenic emission rates.

593   Inorganic nitrate was the second largest component in winter (17%) but accounted for only

594   ~0.4% of NR-PM$_1$ mass in summer; SO$_4^{2-}$ was the third and second largest component in

595   winter (20%) and summer (31%), respectively. ON, on average accounted for ~15 and ~37 %

596   of OA during winter and summer campaign, respectively. The summertime ON correlated very

597   well with LO-OOA and concurrently peaked at nighttime. It is likely that ON from NO$_3$·

598   -initiated oxidation of BVOC in the forested northeastern Houston contributed greatly to

599   nighttime LO-OOA in summer.

600   Contributions of factors to wintertime and summertime OA show distinct differences. For

601   wintertime OA, on average, BBOA, MO-OOA, and COA made similar contributions of 24%,

602   23% and 22% to total OA mass, respectively. LO-OOA accounted for 18% of OA mass,

603   followed by HOA. In the summer, LO-OOA represented the largest fraction of the OA mass, 53%

604   on average. The second largest contributor was MO-OOA (24%). Together, POA constituted

605   more than half of OA mass (59%) in winter, while it accounted for 23% of OA mass in summer,

606   highlighting the enhanced impact of primary emissions on OA level during wintertime.

607   Secondary aerosols account for ~76% and 89% of NR-PM$_1$ mass in winter and summer,

608   respectively, indicating NR-PM$_1$ mass was likely driven mostly by secondary aerosol

609   formation.

610   The two proxies of SOA (LO-OOA and MO-OOA) presented seasonal differences in their

611   spectral patterns, oxidation degrees and contributions to SOA. MO-OOA showed a higher

612   contribution to SOA than LO-OOA in winter (56% vs. 44%). In contrast, LO-OOA dominated

613   SOA in summer (69%). Our results indicate that both photochemical and aqueous-phase

614   chemistry played important roles in the formation of MO-OOA and LO-OOA. Aqueous-phase

615   processing likely has strong positive impact on the formation of MO-OOA in the two seasons,

616   especially in winter. The relationships between MO-OOA and LWC were 0.0076 and 0.0045 μg

617   MO-OOA μg^{-1} LWC during winter and summer, respectively. Wet removal likely limits

618   MO-OOA when LWC exceeds 100 μg m^{-3} in winter. Interestingly, the relative importance of

619   aqueous-phase chemistry versus photochemistry in processing LO-OOA was dependent on RH.

620   Aqueous-phase processing likely facilitated the local formation of wintertime LO-OOA at low

621   LWC level (<17.5 μg m^{-3}, RH<80%), with a stronger dependence (0.033 μg LO-OOA μg^{-1}

622   LWC) than MO-OOA. In summer, the formation of LO-OOA was enhanced by aqueous-phase

623   processing at relatively high LWC level (>6.25 μg m^{-3}, RH>80%) with a slope of 0.0526 μg

624   LO-OOA μg^{-1} LWC, while LO-OOA was likely transported non-aqueous regional OOA when

625   LWC < 6.25 μg m^{-3}. These increases of OOA in response to LWC were greatly enhanced

626   during nighttime. Aqueous-phase chemistry also was predominant in the formation of

627   summertime LO-OOA at low atmospheric oxidative capacity (O_x < 20 ppb). In general,

628   summertime LO-OOA showed a much stronger response to O_x than did MO-OOA, with a slope

629   of 0.0299 μg LO-OOA ppb^{-1} O_x. LO-OOA in summer was elevated by nearly 1.2 μg m^{-3} as a

630   ~20 μg change in LWC, which is equivalent to a 40 ppb change in O_x.

631

632   **Acknowledgments**

640

641   *Author contribution*. Qili Dai performed the data analysis and wrote the manuscript. Robert J.

642   Griffin and Yinchang Feng assisted heavily with manuscript development and editing. Henry

643   W. Wallace, Alexander A.T. Bui, James H. Flynn, Barry L. Lefer contributed to data collection

644   during the field campaigns. Benjamin C. Schulze, Henry W. Wallace, Alexander A.T. Bui and

645   Nancy P. Sanchez contributed with data analysis. Xiaohui Bi, Benjamin C. Schulze, Alexander

646   A.T. Bui, Fangzhou Guo, Nancy P. Sanchez, James H. Flynn provided helpful comments and

647   edits.

Atmospheric
Chemistry
and Physics
Discussions

648

Competing interests. The authors declare that they have no conflict of interest.

650

References

Allen, D. T., and Fraser, M.: An overview of the Gulf Coast Aerosol Research and Characterization Study: The Houston Fine Particulate Matter Supersite, J. Air Waste Manage., 56, 456-466, http://doi.org/10.1080/10473289.2006.10464514, 2006.

Atkinson, D. B., Massoli, P., O'Neill, N. T., Quinn, P. K., Brooks, S. D., and Lefer, B.: Comparison of in situ and columnar aerosol spectral measurements during TexAQS-GoMACCS 2006: testing parameterizations for estimating aerosol fine mode properties, Atmos. Chem. Phys., 10, 51-61, http://doi.org/10.5194/acp-10-51-2010, 2010.

Ayres, B. R., Allen, H. M., Draper, D. C., Brown, S. S., Wild, R. J., Jimenez, J. L., Day, D. A., Campuzano-Jost, P., Hu, W., de Gouw, J., Koss, A., Cohen, R. C., Duffey, K. C., Romer, P., Baumann, K., Edgerton, E., Takahama, S., Thornton, J. A., Lee, B. H., Lopez-Hilfiker, F. D., Mohr, C., Wennberg, P. O., Nguyen, T. B., Teng, A., Goldstein, A. H., Olson, K., and Fry, J. L.: Organic nitrate aerosol formation via NO_3 + biogenic volatile organic compounds in the southeastern United States, Atmos. Chem. Phys., 15, 13377-13392, http://doi.org/10.5194/acp-15-13377-2015, 2015.

Bahreini, R., Ervens, B., Middlebrook, A. M., Warneke, C., de Gouw, J. A., DeCarlo, P. F., Jimenez, J. L., Brock, C. A., Neuman, J. A., Ryerson, T. B., Stark, H., Atlas, E., Brioude, J., Fried, A., Holloway, J. S., Peischl, J., Richter, D., Walega, J., Weibring, P., Wollny, A. G., and Fehsenfeld, F. C.: Organic aerosol formation in urban and industrial plumes near Houston and Dallas, Texas, J. Geophys. Res., 114, D00f16, http://doi.org/10.1029/2008jd011493, 2009.

Barnes, I., Hjorth, J., and Mihalopoulos, N.: Dimethyl sulfide and dimethyl sulfoxide and their oxidation in the atmosphere, Chem. Rev., 106, 940-975, http://doi.org/10.1021/cr020529+, 2006.

Bates, T. S., Quinn, P. K., Coffman, D., Schulz, K., Covert, D. S., Johnson, J. E., Williams, E. J., Lerner, B. M., Angevine, W. M., Tucker, S. C., Brewer, W. A., and Stohl, A.: Boundary layer aerosol chemistry during TexAQS/GoMACCS 2006: Insights into aerosol sources and transformation processes, J. Geophys. Res., 113, D00f01,

679   http://doi.org/10.1029/2008jd010023, 2008.

680   Bean, J. K., Faxon, C. B., Leong, Y. J., Wallace, H. W., Cevik, B. K., Ortiz, S., Canagaratna, M.

681   R., Usenko, S., Sheesley, R. J., Griffin, R. J., and Hildebrandt, L: Composition and sources

682   of particulate matter measured near Houston, TX; Anthropogenic-biogenic interactions,

683   Atmos., 7, 73, https://doi.org/10.3390/atmos7050073, 2016

684   Berkemeier, T., Ammann, M., Mentel, T. F., Poschl, U., and Shiraiwa, M.: Organic Nitrate

685   Contribution to New Particle Formation and Growth in Secondary Organic Aerosols from

686   alpha-Pinene   Ozonolysis,   Environ.   Sci.   Technol.,   50,   6334-6342,

687   http://doi.org/10.1021/acs.est.6b00961, 2016.

688   Brown, S. S., Dube, W. P., Bahreini, R., Middlebrook, A. M., Brock, C. A., Warneke, C., de

689   Gouw, J. A., Washenfelder, R. A., Atlas, E., Peischl, J., Ryerson, T. B., Holloway, J. S.,

690   Schwarz, J. P., Spackman, R., Trainer, M., Parrish, D. D., Fehshenfeld, F. C., and

691   Ravishankara, A. R.: Biogenic VOC oxidation and organic aerosol formation in an urban

692   nocturnal boundary layer: aircraft vertical profiles in Houston, TX, Atmos. Chem. Phys.,

693   13, 11317-11337, http://doi.org/10.5194/acp-13-11317-2013, 2013.

694   Budisulistiorini, S. H., Baumann, K., Edgerton, E. S., Bairai, S. T., Mueller, S., Shaw, S. L.,

695   Knipping, E. M., Gold, A., and Surratt, J. D.: Seasonal characterization of submicron

696   aerosol chemical composition and organic aerosol sources in the southeastern United States:

697   Atlanta, Georgia,and Look Rock, Tennessee, Atmos. Chem. Phys., 16, 5171-5189,

698   http://doi.org/10.5194/acp-16-5171-2016, 2016.

699   Canagaratna, M. R., Jayne, J. T., Jimenez, J. L., Allan, J. D., Alfarra, M. R., Zhang, Q., Onasch,

700   T. B., Drewnick, F., Coe, H., Middlebrook, A., Delia, A., Williams, L. R., Trimborn, A. M.,

701   Northway, M. J., DeCarlo, P. F., Kolb, C. E., Davidovits, P., and Worsnop, D. R.: Chemical

702   and microphysical characterization of ambient aerosols with the aerodyne aerosol mass

703   spectrometer, Mass Spectrom. Rev., 26, 185-222, http://doi.org/10.1002/mas.20115, 2007.

704   Canagaratna, M. R., Jimenez, J. L., Kroll, J. H., Chen, Q., Kessler, S. H., Massoli, P.,

705   Hildebrandt Ruiz, L., Fortner, E., Williams, L. R., Wilson, K. R., Surratt, J. D., Donahue, N.

706   M., Jayne, J. T., and Worsnop, D. R.: Elemental ratio measurements of organic compounds

707   using aerosol mass spectrometry: characterization, improved calibration, and implications,

708   Atmos. Chem. Phys., 15, 253-272, http://doi.org/10.5194/acp-15-253-2015, 2015.

709   Chakraborty, A., Bhattu, D., Gupta, T., Tripathi, S. N., and Canagaratna, M. R.: Real-time

710   measurements of ambient aerosols in a polluted Indian city: Sources, characteristics, and

711   processing of organic aerosols during foggy and nonfoggy periods, J. Geophys. Res., 120,

712   9006-9019, http://doi.org/10.1002/2015jd023419, 2015.

713 Chang, R. Y. W., Slowik, J. G., Shantz, N. C., Vlasenko, A., Liggio, J., Sjostedt, S. J., Leaitch,
714   W. R., and Abbatt, J. P. D.: The hygroscopicity parameter (kappa) of ambient organic
715   aerosol at a field site subject to biogenic and anthropogenic influences: relationship to
716   degree of aerosol oxidation, Atmos. Chem. Phys., 10, 5047-5064,
717   http://doi.org/10.5194/acp-10-5047-2010, 2010.

718 Chhabra, P. S., Flagan, R. C., and Seinfeld, J. H.: Elemental analysis of chamber organic
719   aerosol using an aerodyne high-resolution aerosol mass spectrometer, Atmos. Chem. Phys.,
720   10, 4111-4131, http://doi.org/10.5194/acp-10-4111-2010, 2010.

721 Cleveland, M. J., Ziemba, L. D., Griffin, R. J., Dibb, J. E., Anderson, C. H., Lefer, B., and
722   Rappengluck, B.: Characterization of urban aerosol using aerosol mass spectrometry and
723   proton nuclear magnetic resonance spectroscopy, Atmos. Environ., 54, 511-518,
724   http://doi.org/10.1016/j.atmosenv.2012.02.074, 2012.

725 Crippa, M., El Haddad, I., Slowik, J. G., DeCarlo, P. F., Mohr, C., Heringa, M. F., Chirico, R.,
726   Marchand, N., Sciare, J., Baltensperger, U., and Prevot, A. S. H.: Identification of marine
727   and continental aerosol sources in Paris using high resolution aerosol mass spectrometry, J.
728   Geophys. Res., 118, 1950-1963, http://doi.org/10.1002/jgrd.50151, 2013a.

729 Crippa, M., DeCarlo, P. F., Slowik, J. G., Mohr, C., Heringa, M. F., Chirico, R., Poulain, L.,
730   Freutel, F., Sciare, J., Cozic, J., Di Marco, C. F., Elsasser, M., Nicolas, J. B., Marchand, N.,
731   Abidi, E., Wiedensohler, A., Drewnick, F., Schneider, J., Borrmann, S., Nemitz, E.,
732   Zimmermann, R., Jaffrezo, J. L., Prevot, A. S. H., and Baltensperger, U.: Wintertime
733   aerosol chemical composition and source apportionment of the organic fraction in the
734   metropolitan area of Paris, Atmos. Chem. Phys., 13, 961-981,
735   http://doi.org/10.5194/acp-13-961-2013, 2013b.

736 de Gouw, J. A., Brock, C. A., Atlas, E. L., Bates, T. S., Fehsenfeld, F. C., Goldan, P. D.,
737   Holloway, J. S., Kuster, W. C., Lerner, B. M., Matthew, B. M., Middlebrook, A. M.,
738   Onasch, T. B., Peltier, R. E., Quinn, P. K., Senff, C. J., Stohl, A., Sullivan, A. P., Trainer, M.,
739   Warneke, C., Weber, R. J., and Williams, E. J.: Sources of particulate matter in the
740   northeastern United States in summer: 1. Direct emissions and secondary formation of
741   organic matter in urban plumes, J. Geophys. Res., 113, D08301,
742   http://doi.org/10.1029/2007jd009243, 2008.

743 DeCarlo, P. F., Kimmel, J. R., Trimborn, A., Northway, M. J., Jayne, J. T., Aiken, A. C., Gonin,
744   M., Fuhrer, K., Horvath, T., Docherty, K. S., Worsnop, D. R., and Jimenez, J. L.:

Atmospheric
Chemistry
and Physics
Discussions

745   Field-deployable, high-resolution, time-of-flight aerosol mass spectrometer, Anal. Chem.,
746   78, 8281-8289, http://doi.org/10.1021/ac061249n, 2006.

747   Duplissy, J., DeCarlo, P. F., Dommen, J., Alfarra, M. R., Metzger, A., Barmpadimos, I., Prevot,
748   A. S. H., Weingartner, E., Tritscher, T., Gysel, M., Aiken, A. C., Jimenez, J. L.,
749   Canagaratna, M. R., Worsnop, D. R., Collins, D. R., Tomlinson, J., and Baltensperger, U.:
750   Relating hygroscopicity and composition of organic aerosol particulate matter, Atmos.
751   Chem. Phys., 11, 1155-1165, http://doi.org/10.5194/acp-11-1155-2011, 2011.

752   Ervens, B., Turpin, B. J., and Weber, R. J.: Secondary organic aerosol formation in cloud
753   droplets and aqueous particles (aqSOA): a review of laboratory, field and model studies,
754   Atmos. Chem. Phys., 11, 11069-11102, http://doi.org/10.5194/acp-11-11069-2011, 2011.

755   Farmer, D. K., Matsunaga, A., Docherty, K. S., Surratt, J. D., Seinfeld, J. H., Ziemann, P. J., and
756   Jimenez, J. L.: Response of an aerosol mass spectrometer to organonitrates and
757   organosulfates and implications for atmospheric chemistry, P. Natl. Acad. Sci. USA, 107,
758   6670-6675, http://doi.org/10.1073/pnas.0912340107, 2010.

759   Fountoukis, C., and Nenes, A.: ISORROPIA II: a computationally efficient thermodynamic
760   equilibrium model for K+-Ca2+-Mg2+-Nh(4)(+)-Na+-SO42--NO3--Cl--H2O aerosols,
761   Atmos. Chem. Phys., 7, 4639-4659, , http://doi.org/10.5194/acp-7-4639-2007, 2007.

762   Fry, J. L., Kiendler-Scharr, A., Rollins, A. W., Wooldridge, P. J., Brown, S. S., Fuchs, H., Dube,
763   W., Mensah, A., dal Maso, M., Tillmann, R., Dorn, H. P., Brauers, T., and Cohen, R. C.:
764   Organic nitrate and secondary organic aerosol yield from NO3 oxidation of beta-pinene
765   evaluated using a gas-phase kinetics/aerosol partitioning model, Atmos. Chem. Phys., 9,
766   1431-1449, http://doi.org/10.5194/acp-9-1431-2009, 2009.

767   Fry, J. L., Draper, D. C., Zarzana, K. J., Campuzano-Jost, P., Day, D. A., Jimenez, J. L., Brown,
768   S. S., Cohen, R. C., Kaser, L., Hansel, A., Cappellin, L., Karl, T., Roux, A. H., Turnipseed,
769   A., Cantrell, C., Lefer, B. L., and Grossberg, N.: Observations of gas- and aerosol-phase
770   organic nitrates at BEACHON-RoMBAS 2011, Atmos. Chem. Phys., 13, 8585-8605,
771   http://doi.org/10.5194/acp-13-8585-2013, 2013.

772   Ge, X., Zhang, Q., Sun, Y., Ruehl, C. R., and Setyan, A.: Effect of aqueous-phase processing on
773   aerosol chemistry and size distributions in Fresno, California, during wintertime, Environ.
774   Chem., 9, 221, http://doi.org/10.1071/en11168, 2012.

775   Gondwe, M., Krol, M., Klaassen, W., Gieskes, W., and de Baar, H.: Comparison of modeled
776   versus measured MSA:nss SO4= ratios: A global analysis, Global Biogeochem. Cy., 18,
777   http://doi.org/10.1029/2003GB002144, 2004.

778   Grantz, D. A., Garner, J. H. B., and Johnson, D. W.: Ecological effects of particulate matter,
779   Environ. Int., 29, 213-239, http://doi.org/10.1016/S0160-4120(02)00181-2, 2003.

780   Guo, H., Xu, L., Bougiatioti, A., Cerully, K. M., Capps, S. L., Hite, J. R., Carlton, A. G., Lee, S.
781   H., Bergin, M. H., Ng, N. L., Nenes, A., and Weber, R. J.: Fine-particle water and pH in the
782   southeastern United States, Atmos. Chem. Phys., 15, 5211-5228,
783   http://doi.org/10.5194/acp-15-5211-2015, 2015.

784   Haman, C. L., Lefer, B., and Morris, G. A.: Seasonal Variability in the Diurnal Evolution of the
785   Boundary Layer in a Near-Coastal Urban Environment, J. Atmos. Ocean Tech., 29,
786   697-710, , http://doi.org/10.1175/Jtech-D-11-00114.1, 2012.

787   Hayes, P. L., Ortega, A. M., Cubison, M. J., Froyd, K. D., Zhao, Y., Cliff, S. S., Hu, W. W.,
788   Toohey, D. W., Flynn, J. H., Lefer, B. L., Grossberg, N., Alvarez, S., Rappenglueck, B.,
789   Taylor, J. W., Allan, J. D., Holloway, J. S., Gilman, J. B., Kuster, W. C., De Gouw, J. A.,
790   Massoli, P., Zhang, X., Liu, J., Weber, R. J., Corrigan, A. L., Russell, L. M., Isaacman, G.,
791   Worton, D. R., Kreisberg, N. M., Goldstein, A. H., Thalman, R., Waxman, E. M., Volkamer,
792   R., Lin, Y. H., Surratt, J. D., Kleindienst, E., Offenberg, J. H., Dusanter, S., Griffith, S.,
793   Stevens, P. S., Brioude, J., Angevine, W. M., and Jimenez, J. L.: Organic aerosol
794   composition and sources in Pasadena, California, during the 2010 CalNex campaign, J.
795   Geophys. Res., 118, 9233-9257, http://doi.org/10.1002/jgrd.50530, 2013.

796   Hennigan, C. J., Bergin, M. H., Dibb, J. E., and Weber, R. J.: Enhanced secondary organic
797   aerosol formation due to water uptake by fine particles, Geophys. Res. Lett., 35, L18801,
798   http://doi.org/10.1029/2008gl035046, 2008.

799   Hu, W. W., Campuzano-Jost, P., Palm, B. B., Day, D. A., Ortega, A. M., Hayes, P. L., Krechmer,
800   J. E., Chen, Q., Kuwata, M., Liu, Y. J., de Sa, S. S., McKinney, K., Martin, S. T., Hu, M.,
801   Budisulistiorini, S. H., Riva, M., Surratt, J. D., St Clair, J. M., Isaacman-Van Wertz, G., Yee,
802   L. D., Goldstein, A. H., Carbone, S., Brito, J., Artaxo, P., de Gouw, J. A., Koss, A.,
803   Wisthaler, A., Mikoviny, T., Karl, T., Kaser, L., Jud, W., Hansel, A., Docherty, K. S.,
804   Alexander, M. L., Robinson, N. H., Coe, H., Allan, J. D., Canagaratna, M. R., Paulot, F.,
805   and Jimenez, J. L.: Characterization of a real-time tracer for isoprene epoxydiols-derived
806   secondary organic aerosol (IEPOX-SOA) from aerosol mass spectrometer measurements,
807   Atmos. Chem. Phys., 15, 11807-11833, http://doi.org/10.5194/acp-15-11807-2015, 2015.

808   Hu, W. W., Hu, M., Hu, W., Jimenez, J. L., Yuan, B., Chen, W. T., Wang, M., Wu, Y. S., Chen,
809   C., Wang, Z. B., Peng, J. F., Zeng, L. M., and Shao, M.: Chemical composition, sources,
810   and aging process of submicron aerosols in Beijing: Contrast between summer and winter,

Atmospheric
Chemistry
and Physics
Discussions

Open Access

EGU

811   J. Geophys. Res., 121, 1955-1977, http://doi.org/10.1002/2015jd024020, 2016.

812   Huang, D. D., Li, Y. J., Lee, B. P., and Chan, C. K.: Analysis of Organic Sulfur Compounds in

813   Atmospheric Aerosols at the HKUST Supersite in Hong Kong using HR-ToF-AMS,

814   Environ. Sci. Technol., 49, 3672-3679, http://doi.org/10.1021/es5056269, 2015.

815   Jimenez, J. L., Canagaratna, M. R., Donahue, N. M., Prevot, A. S. H., Zhang, Q., Kroll, J. H.,

816   DeCarlo, P. F., Allan, J. D., Coe, H., Ng, N. L., Aiken, A. C., Docherty, K. S., Ulbrich, I.

817   M., Grieshop, A. P., Robinson, A. L., Duplissy, J., Smith, J. D., Wilson, K. R., Lanz, V. A.,

818   Hueglin, C., Sun, Y. L., Tian, J., Laaksonen, A., Raatikainen, T., Rautiainen, J., Vaattovaara,

819   P., Ehn, M., Kulmala, M., Tomlinson, J. M., Collins, D. R., Cubison, M. J., Dunlea, E. J.,

820   Huffman, J. A., Onasch, T. B., Alfarra, M. R., Williams, P. I., Bower, K., Kondo, Y.,

821   Schneider, J., Drewnick, F., Borrmann, S., Weimer, S., Demerjian, K., Salcedo, D., Cottrell,

822   L., Griffin, R., Takami, A., Miyoshi, T., Hatakeyama, S., Shimono, A., Sun, J. Y., Zhang, Y.

823   M., Dzepina, K., Kimmel, J. R., Sueper, D., Jayne, J. T., Herndon, S. C., Trimborn, A. M.,

824   Williams, L. R., Wood, E. C., Middlebrook, A. M., Kolb, C. E., Baltensperger, U., and

825   Worsnop, D. R.: Evolution of Organic Aerosols in the Atmosphere, Science, 326,

826   1525-1529, http://doi.org/10.1126/science.1180353, 2009.

827   Kim, H., Zhang, Q., Bae, G. N., Kim, J. Y., and Lee, S. B.: Sources and atmospheric processing

828   of winter aerosols in Seoul, Korea: insights from real-time measurements using a

829   high-resolution aerosol mass spectrometer, Atmos. Chem. Phys., 17, 2009-2033,

830   http://doi.org/10.5194/acp-17-2009-2017, 2017.

831   Kuwata, M., Zorn, S. R., and Martin, S. T.: Using Elemental Ratios to Predict the Density of

832   Organic Material Composed of Carbon, Hydrogen, and Oxygen, Environ. Sci. Technol., 46,

833   787-794, http://doi.org/10.1021/es202525q, 2012.

834   Lefer, B., Rappengluck, B., Flynn, J., and Haman, C.: Photochemical and meteorological

835   relationships during the Texas-II Radical and Aerosol Measurement Project (TRAMP),

836   Atmos. Environ., 44, 4005-4013, http://doi.org/10.1016/j.atmosenv.2010.03.011, 2010.

837   Leong, Y. J., Sanchez, N. P., Wallace, H. W., Cevik, B. K., Hernandez, C. S., Han, Y., Flynn, J.

838   H., Massoli, P., Floerchinger, C., Fortner, E. C., Herndon, S., Bean, J. K., Hildebrandt Ruiz,

839   L., Jeon, W., Choi, Y., Lefer, B., and Griffin, R. J.: Overview of surface measurements and

840   spatial characterization of submicrometer particulate matter during the DISCOVER-AQ

841   2013 campaign in Houston, TX, J. Air Waste Manage., 67, 854-872,

842   http://doi.org/10.1080/10962247.2017.1296502, 2017.

843   Li, J. Y., Cleveland, M., Ziemba, L. D., Griffin, R. J., Barsanti, K. C., Pankow, J. F., and Ying,

Atmospheric
Chemistry
and Physics
Discussions

Open Access

EGU

844   Q.: Modeling regional secondary organic aerosol using the Master Chemical Mechanism,

845   Atmos. Environ., 102, 52-61, http://doi.org/10.1016/j.atmosenv.2014.11.054, 2015.

846 Lim, Y. B., Tan, Y., Perri, M. J., Seitzinger, S. P., and Turpin, B. J.: Aqueous chemistry and its

847   role in secondary organic aerosol (SOA) formation, Atmos. Chem. Phys., 10, 10521-10539,

848   http://doi.org/10.5194/acp-10-10521-2010, 2010.

849 Liu, J. B., Rhland, K. M., Chen, J. H., Xu, Y. Y., Chen, S. Q., Chen, Q. M., Huang, W., Xu, Q.

850   H., Chen, F. H., and Smol, J. P.: Aerosol-weakened summer monsoons decrease lake

851   fertilization on the Chinese Loess Plateau, Nat. Clim. Change, 7, 190-194,

852   http://10.1038/Nclimate3220, 2017.

853 Mao, J. Q., Ren, X. R., Chen, S. A., Brune, W. H., Chen, Z., Martinez, M., Harder, H., Lefer, B.,

854   Rappengluck, B., Flynn, J., and Leuchner, M.: Atmospheric oxidation capacity in the

855   summer of Houston 2006: Comparison with summer measurements in other metropolitan

856   studies, Atmos. Environ., 44, 4107-4115, http://doi.org/10.1016/j.atmosenv.2009.01.013,

857   2010.

858 McKeen, S., Grell, G., Peckham, S., Wilczak, J., Djalalova, I., Hsie, E. Y., Frost, G., Peischl, J.,

859   Schwarz, J., Spackman, R., Holloway, J., de Gouw, J., Warneke, C., Gong, W., Bouchet, V.,

860   Gaudreault, S., Racine, J., McHenry, J., McQueen, J., Lee, P., Tang, Y., Carmichael, G. R.,

861   and Mathur, R.: An evaluation of real-time air quality forecasts and their urban emissions

862   over eastern Texas during the summer of 2006 Second Texas Air Quality Study field study,

863   J. Geophys. Res., 114, D00f11, http://doi.org/10.1029/2008JD011697, 2009.

864 Middlebrook, A. M., Bahreini, R., Jimenez, J. L., and Canagaratna, M. R.: Evaluation of

865   Composition-Dependent Collection Efficiencies for the Aerodyne Aerosol Mass

866   Spectrometer using Field Data, Aerosol Sci. Tech., 46, 258-271,

867   http://doi.org/10.1080/02786826.2011.620041, 2012.

868 Olaguer, E. P., Kolb, C. E., Lefer, B., Rappenglueck, B., Zhang, R. Y., and Pinto, J. P.:

869   Overview of the SHARP campaign: Motivation, design, and major outcomes, J. Geophys.

870   Res., 119, 2597-2610, http://doi.org/10.1002/2013jd019730, 2014.

871 Paatero, P., Hopke, P. K., Song, X. H., and Ramadan, Z.: Understanding and controlling

872   rotations in factor analytic models, Chemometr. Intell. Lab, 60, 253-264,

873   http://doi.org/10.1016/S0169-7439(01)00200-3, 2002.

874 Paatero, P., and Tapper, U.: Positive matrix factorization: A non-negative factor model with

875   optimal utilization of error estimates of data values, Environmetrics, 5, 111-126,

876   https://doi.org/10.1002/env.3170050203, 1994.

Atmospheric
Chemistry
and Physics
Discussions

877   Parrish, D. D.,   Allen, D. T., Bates, T. S., Estes, M., Fehsenfeld, F. C., Feingold, G., Ferrare,
878   R., Hardesty, R. M., Meagher, J. F., Nielsen-Gammon, J. W., Pierce, R. B., Ryerson, T. B.,
879   Seinfeld, J. H., and Williams, E. J.: Overview of the Second Texas Air Quality Study
880   (TexAQS II) and the Gulf of Mexico Atmospheric Composition and Climate Study
881   (GoMACCS), J. Geophys. Res., 114, D00f13, http://doi.org/10.1029/2009jd011842, 2009.

882   Petters, M. D., and Kreidenweis, S. M.: A single parameter representation of hygroscopic
883   growth and cloud condensation nucleus activity, Atmos. Chem. Phys., 7, 1961-1971, ,
884   http://doi.org/10.5194/acp-7-1961-2007, 2007.

885   Petters, M. D., Wex, H., Carrico, C. M., Hallbauer, E., Massling, A., McMeeking, G. R.,
886   Poulain, L., Wu, Z., Kreidenweis, S. M., and Stratmann, F.: Towards closing the gap
887   between hygroscopic growth and activation for secondary organic aerosol - Part 2:
888   Theoretical   approaches,   Atmos.   Chem.   Phys.,   9,   3999-4009,
889   http://doi.org/10.5194/acp-9-3999-2009, 2009.

890   Prenni, A. J., Petters, M. D., Kreidenweis, S. M., DeMott, P. J., and Ziemann, P. J.: Cloud
891   droplet activation of secondary organic aerosol, J. Geophys. Res., 112, D10223,
892   http://doi.org/10.1029/2006jd007963, 2007.

893   Racherla, P. N., and Adams, P. J.: Sensitivity of global tropospheric ozone and fine particulate
894   matter   concentrations   to   climate   change,   J.   Geophys.   Res.,   111,
895   https://doi.org/10.1029/2005JD006939, 2006.

896   Rollins, A. W., Smith, J. D., Wilson, K. R., and Cohen, R. C.: Real Time In Situ Detection of
897   Organic Nitrates in Atmospheric Aerosols, Environ. Sci. Technol., 44, 5540-5545,
898   http://doi.org/10.1021/es100926x, 2010.

899   Rollins, A. W., Browne, E. C., Min, K. E., Pusede, S. E., Wooldridge, P. J., Gentner, D. R.,
900   Goldstein, A. H., Liu, S., Day, D. A., Russell, L. M., and Cohen, R. C.: Evidence for NOx
901   Control   over   Nighttime   SOA   Formation,   Science,   337,   1210-1212,
902   http://doi.org/10.1126/science.1221520, 2012.

903   Russell, L. M., Takahama, S., Liu, S., Hawkins, L. N., Covert, D. S., Quinn, P. K., and Bates, T.
904   S.: Oxygenated fraction and mass of organic aerosol from direct emission and atmospheric
905   processing measured on the R/V Ronald Brown during TEXAQS/GoMACCS 2006, J.
906   Geophys. Res., 114, D00F05, http://doi.org/10.1029/2008JD011275, 2009.

907   Schulze, B. C., Wallace, H. W., Bui, A. T., Flynn, J. H., Erickson, M. H., Alvarez, S., Dai, Q.,
908   Usenko, S., Sheesley, R. J., and Griffin, R. J.: The impacts of regional shipping emissions
909   on the chemical characteristics of coastal submicron aerosols near Houston, TX, Atmos.

Atmospheric
Chemistry
and Physics
Discussions

910   Chem. Phys., 18, 14217-14241, http://doi.org/10.5194/acp-18-14217-2018, 2018.

911   Setyan, A., Zhang, Q., Merkel, M., Knighton, W. B., Sun, Y., Song, C., Shilling, J. E., Onasch,

912   T. B., Herndon, S. C., Worsnop, D. R., Fast, J. D., Zaveri, R. A., Berg, L. K., Wiedensohler,

913   A., Flowers, B. A., Dubey, M. K., and Subramanian, R.: Characterization of submicron

914   particles influenced by mixed biogenic and anthropogenic emissions using high-resolution

915   aerosol mass spectrometry: results from CARES, Atmos. Chem. Phys., 12, 8131-8156,

916   http://doi.org/10.5194/acp-12-8131-2012, 2012.

917   Sullivan, A. P., Hodas, N., Turpin, B. J., Skog, K., Keutsch, F. N., Gilardoni, S., Paglione, M.,

918   Rinaldi, M., Decesari, S., Facchini, M. C., Poulain, L., Herrmann, H., Wiedensohler, A.,

919   Nemitz, E., Twigg, M. M., and Collett Jr, J. L.: Evidence for ambient dark aqueous SOA

920   formation in the Po Valley, Italy, Atmos. Chem. Phys., 16, 8095-8108,

921   http://doi.org/10.5194/acp-16-8095-2016, 2016.

922   Sun, Y. L., Zhang, Q., Schwab, J. J., Demerjian, K. L., Chen, W. N., Bae, M. S., Hung, H. M.,

923   Hogrefe, O., Frank, B., Rattigan, O. V., and Lin, Y. C.: Characterization of the sources and

924   processes of organic and inorganic aerosols in New York city with a high-resolution

925   time-of-flight aerosol mass spectrometer, Atmos. Chem. Phys., 11, 1581-1602,

926   https://doi.org/10.5194/acp-11-1581-2011, 2011.

927   Sun, Y. L., Du, W., Fu, P. Q., Wang, Q. Q., Li, J., Ge, X. L., Zhang, Q., Zhu, C. M., Ren, L. J.,

928   Xu, W. Q., Zhao, J., Han, T. T., Worsnop, D. R., and Wang, Z. F.: Primary and secondary

929   aerosols in Beijing in winter: sources, variations and processes, Atmos. Chem. Phys., 16,

930   8309-8329, http://doi.org/10.5194/acp-16-8309-2016, 2016.

931   Surratt, J. D., Gomez-Gonzalez, Y., Chan, A. W. H., Vermeylen, R., Shahgholi, M., Kleindienst,

932   T. E., Edney, E. O., Offenberg, J. H., Lewandowski, M., Jaoui, M., Maenhaut, W., Claeys,

933   M., Flagan, R. C., and Seinfeld, J. H.: Organosulfate formation in biogenic secondary

934   organic aerosol, J. Phys. Chem. A, 112, 8345-8378, http://doi.org/10.1021/jp802310p,

935   2008.

936   Tai, A. P. K., Mickley, L. J., and Jacob, D. J.: Correlations between fine particulate matter

937   (PM2.5) and meteorological variables in the United States: Implications for the sensitivity

938   of   PM2.5   to   climate   change,   Atmos.   Environ.,   44,   3976-3984,

939   http://10.1016/j.atmosenv.2010.06.060, 2010.

940   Takegawa, N., Miyakawa, T., Watanabe, M., Kondo, Y., Miyazaki, Y., Han, S., Zhao, Y., van

941   Pinxteren, D., Bruggemann, E., Gnauk, T., Herrmann, H., Xiao, R., Deng, Z., Hu, M., Zhu,

942   T., and Zhang, Y.: Performance of an Aerodyne Aerosol Mass Spectrometer (AMS) during

943   Intensive Campaigns in China in the Summer of 2006, Aerosol Sci. Tech., 43, 189-204,

944   https://doi.org/10.1080/02786820802582251, 2009.

945   Ulbrich, I. M., Canagaratna, M. R., Zhang, Q., Worsnop, D. R., and Jimenez, J. L.:

946   Interpretation of organic components from Positive Matrix Factorization of aerosol mass

947   spectrometric   data,   Atmos.   Chem.   Phys.,   9,   2891-2918,

948   https://doi.org/10.5194/acp-9-2891-2009, 2009.

949   United States Environmental Protection Agency. National Ambient Air Quality Standards for

950   Particulate Matter, Fed. Reg., 78, 3085–3287, 2013.

951   Wallace, H. W., Sanchez, N. P., Flynn, J. H., Erickson, M. H., Lefer, B. L., and Griffin, R. J.:

952   Source apportionment of particulate matter and trace gases near a major refinery near the

953   Houston   Ship   Channel,   Atmos.   Environ.,   173,   16-29,

954   https://doi.org/10.1016/j.atmosenv.2017.10.049, 2018.

955   Watson, J. G.: Visibility: Science and regulation, J. Air Waste Manage., 52, 628-713,

956   http://doi10.1080/10473289.2002.10470813, 2002.

957   Wood, E. C., Canagaratna, M. R., Herndon, S. C., Onasch, T. B., Kolb, C. E., Worsnop, D. R.,

958   Kroll, J. H., Knighton, W. B., Seila, R., Zavala, M., Molina, L. T., DeCarlo, P. F., Jimenez,

959   J. L., Weinheimer, A. J., Knapp, D. J., Jobson, B. T., Stutz, J., Kuster, W. C., and Williams,

960   E. J.: Investigation of the correlation between odd oxygen and secondary organic aerosol in

961   Mexico   City   and   Houston,   Atmos.   Chem.   Phys.,   10,   8947-8968,

962   http://doi.org/10.5194/acp-10-8947-2010, 2010.

963   Xu, L., Suresh, S., Guo, H., Weber, R. J., and Ng, N. L.: Aerosol characterization over the

964   southeastern United States using high-resolution aerosol mass spectrometry: spatial and

965   seasonal variation of aerosol composition and sources with a focus on organic nitrates,

966   Atmos. Chem. Phys., 15, 7307-7336, http://doi.org/10.5194/acp-15-7307-2015, 2015.

967   Xu, W. Q., Han, T. T., Du, W., Wang, Q. Q., Chen, C., Zhao, J., Zhang, Y. J., Li, J., Fu, P. Q.,

968   Wang, Z. F., Worsnop, D. R., and Sun, Y. L.: Effects of Aqueous-Phase and Photochemical

969   Processing on Secondary Organic Aerosol Formation and Evolution in Beijing, China,

970   Environ. Sci. Technol., 51, 762-770, http://doi.org/10.1021/acs.est.6b04498, 2017.

971   Ying, Q., Li, J. Y., and Kota, S. H.: Significant Contributions of Isoprene to Summertime

972   Secondary Organic Aerosol in Eastern United States, Environ. Sci. Technol., 49,

973   7834-7842, http://doi.org/10.1021/acs.est.5b02514, 2015.

974   Zhang, Q., Jimenez, J. L., Canagaratna, M. R., Ulbrich, I. M., Ng, N. L., Worsnop, D. R., and

975   Sun, Y. L.: Understanding atmospheric organic aerosols via factor analysis of aerosol mass

Atmospheric
Chemistry
and Physics
Discussions

Open Access

EGU

976   spectrometry: a   review,   Anal.   Bioanal.   Chem.,   401,   3045-3067,
977   https://doi.org/10.1007/s00216-011-5355-y, 2011.

978   Zhang, Q. J., Beekmann, M., Freney, E., Sellegri, K., Pichon, J. M., Schwarzenboeck, A.,
979   Colomb, A., Bourrianne, T., Michoud, V., and Borbon, A.: Formation of secondary organic
980   aerosol in the Paris pollution plume and its impact on surrounding regions, Atmos. Chem.
981   Phys., 15, 13973-13992, http://doi.org/10.5194/acp-15-13973-2015, 2015.

982   Zhu, Q., He, L. Y., Huang, X. F., Cao, L. M., Gong, Z. H., Wang, C., Zhuang, X., and Hu, M.:
983   Atmospheric aerosol compositions and sources at two national background sites in
984   northern   and   southern   China,   Atmos.   Chem.   Phys.,   16,   10283-10297,
985   http://doi.org/10.5194/acp-16-10283-2016, 2016.

986   Zorn, S. R., Drewnick, F., Schott, M., Hoffmann, T., and Borrmann, S.: Characterization of the
987   South Atlantic marine boundary layer aerosol using an aerodyne aerosol mass spectrometer,
988   Atmos. Chem. Phys., 8, 4711-4728, http://doi.org/10.5194/acp-8-4711-2008, 2008.

989
990
991

992   **Table 1** Statistics of meteorological parameters, gas-phase pollutants, NR-PM$_1$ species, and PMF OA

993   factors for the winter and summer campaigns at UHSL.

Variables		Season	Ave. value ± 1 SD	Minimum value	Maximum value
Meteorological parameters	Temp (˚C)	Winter	9.3 ± 6.0	0.7	25.9
		Summer	23.6 ± 3.8	12.2	33.1
	RH (%)	Winter	76 ± 18	23	99
		Summer	72 ± 19	21	98
	WS (m s^{-1})	Winter	2.1 ± 1.4	6.8×10^{-3}	9.4
		Summer	2.1 ± 1.2	9.0×10^{-3}	6.7
	Radiometer (W m^{-2})	Winter	0.6 ± 0.9	0.02	3.6
		Summer	1.1 ± 1.3	0.02	4.6
Gas-phase pollutants (ppb)	O$_3$	Winter	23.0 ± 12.6	0.12	53.0
		Summer	34.9 ± 15.3	0.02	75.9
	CO	Winter	238.7 ± 71.9	98.5	621.1
		Summer	168.3 ± 75.5	103.6	1110.2
	SO$_2$	Winter	1.0 ± 1.9	5.7×10^{-3}	29.5
		Summer	0.7 ± 1.7	2.8×10^{-3}	30.9
	NO	Winter	4.3 ± 6.4	2.0×10^{-3}	74.9
		Summer	1.3 ± 4.6	0.01	68.1
	NO$_2$	Winter	12.5 ± 9.7	0.8	101.2
		Summer	4.6 ± 6.4	0.2	44.4
	NO$_y$	Winter	22.9 ± 19.6	2.8	210.9
		Summer	8.6 ± 11.9	1.3	123.9
NR-PM$_1$ species (μg m^{-3})	OA	Winter	2.3 ± 1.4	0.42	9.4
		Summer	1.7 ± 1.4	0.27	12.3
	Sulfate	Winter	1.4 ± 0.8	0.05	3.4
		Summer	1.3 ± 0.6	0.02	5.6
	Nitrate	Winter	1.4 ± 1.4	0.02	6.9
		Summer	0.08 ± 0.1	0.01	0.9
	Ammonium	Winter	0.9 ± 0.6	BDL[a]	2.8
		Summer	0.5 ± 0.2	0.02	1.8
	Chloride	Winter	0.06 ± 0.09	BDL	1.1
		Summer	0.02 ± 0.02	BDL	0.5
OA factors (μg m^{-3})	HOA	Winter	0.4 ± 0.4	0[b]	8.6
		Summer	0.3 ± 0.8	0	10.9
	BBOA	Winter	0.7 ± 0.7	0	3.7
		Summer	0.2 ± 0.4	0	5.4
	COA	Winter	0.7 ± 0.6	0	4.8
	LO-OOA	Winter	0.6 ± 0.6	0	2.1
		Summer	1.2 ± 1.3	0	6.7
	MO-OOA	Winter	0.7 ± 0.4	0	1.8
		Summer	0.6 ± 0.3	0	1.6

994   [a]BDL: below detection limit; [b]Statistically determined factor concentrations with values below 1.0x10^{-3} are listed

995   as 0.

996

Atmospheric
Chemistry
and Physics
Discussions

Open Access

EGU

997 **Table** 2 Correlation (r) of OOA mass spectra with previously published spectral database.
998 (http://cires1.colorado.edu/jimenez-group/HRAMSsd/)

Factor	Winter		Summer		Reference
	MO-OOA	LO-OOA	MO-OOA	LO-OOA	
aq-OOA[a]	**0.96**	0.75	**0.96**	**0.95**	Sun et al., 2016
MO-OOA	0.85	0.87	0.89	0.77	Setyan et al., 2012
MO-OOA	0.98	0.92	0.98	0.60	Hu et al., 2015
LV-OOA	0.97	0.91	0.98	0.62	Crippa et al., 2013a
SV-OOA	0.65	0.70	0.70	0.78	Crippa et al., 2013a
LO-OOAI, Biogenic-origin	0.83	0.84	0.86	0.76	Hu et al., 2015
LO-OOAII, Anthropogenic-origin	0.78	0.80	0.82	0.74	Hu et al., 2015

999 [a]aq-OOA is an aqueous-phase-processed SOA reported by Sun et al. (2016); LV=less volatility; SV=semi-volatile.

1000

Atmospheric
Chemistry
and Physics
Discussions
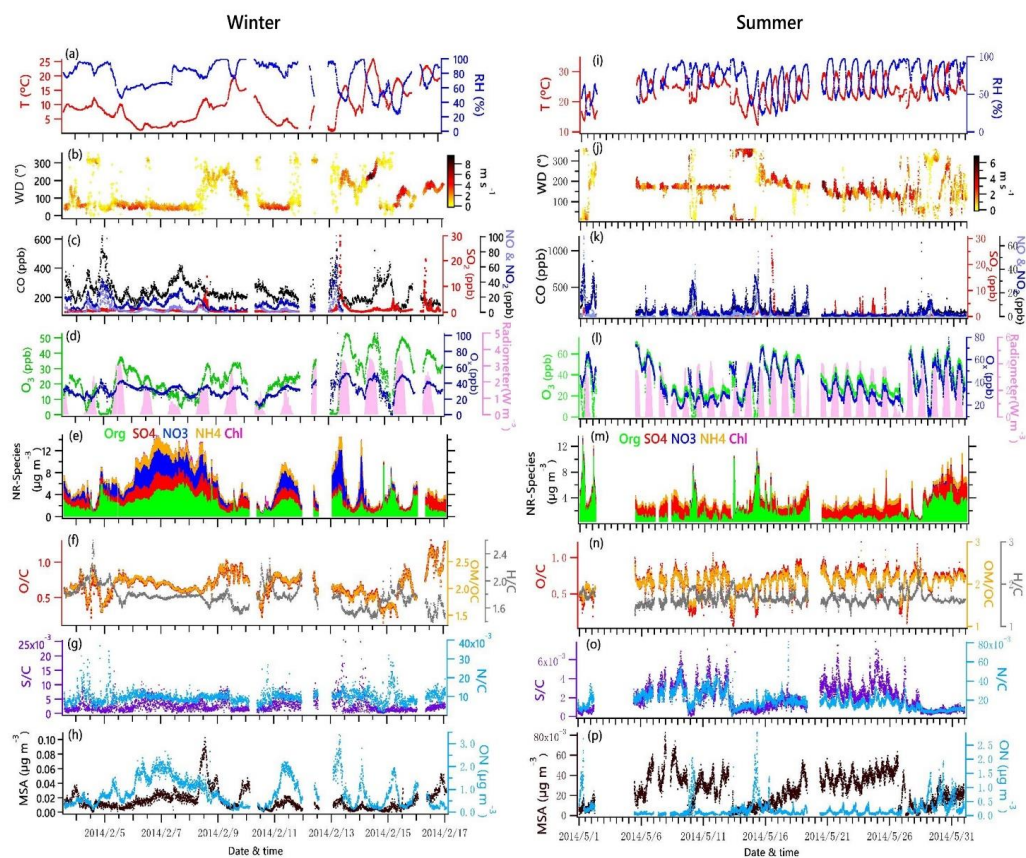
Figure 1. Time series of data collected at UHSL in Houston during the sampling periods in winter and summer 2014. Time series of 5-min average campaign data for **(a, i)** ambient temperature (T) and relative humidity (RH); **(b, j)** wind direction (WD), with colors showing different wind speeds (WS); **(c, k)** CO, SO_2, NO and NO_2; **(d, l)** O_3, O_x (NO_2+O_3) and solar radiometer; **(e, m)** NR-PM_1 species, including OA, NO_3^-, SO_4^{2-}, NH_4^+, and Cl^-; **(f, n)** O/C, OM/OC, and H/C of OA; **(g, o)** N/C and S/C ratios of OA; and **(h, p)** estimated MSA and ON concentrations.
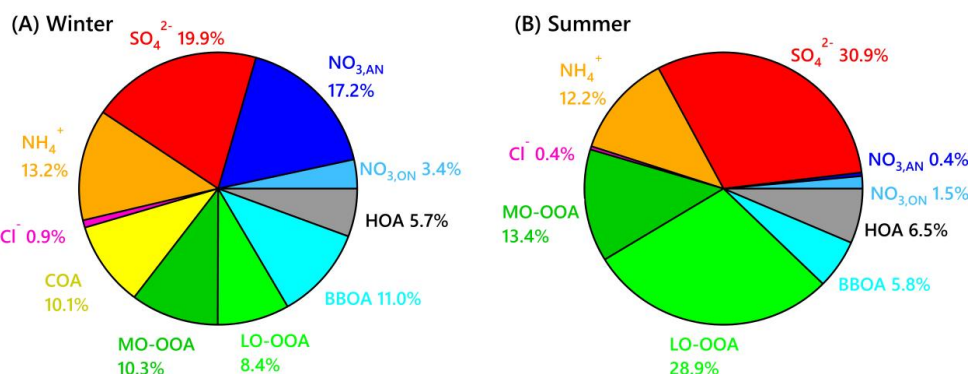
Figure 2. Average composition of NR-PM$_1$ species during the winter (**A**) and summer campaign (**B**) at UHSL.
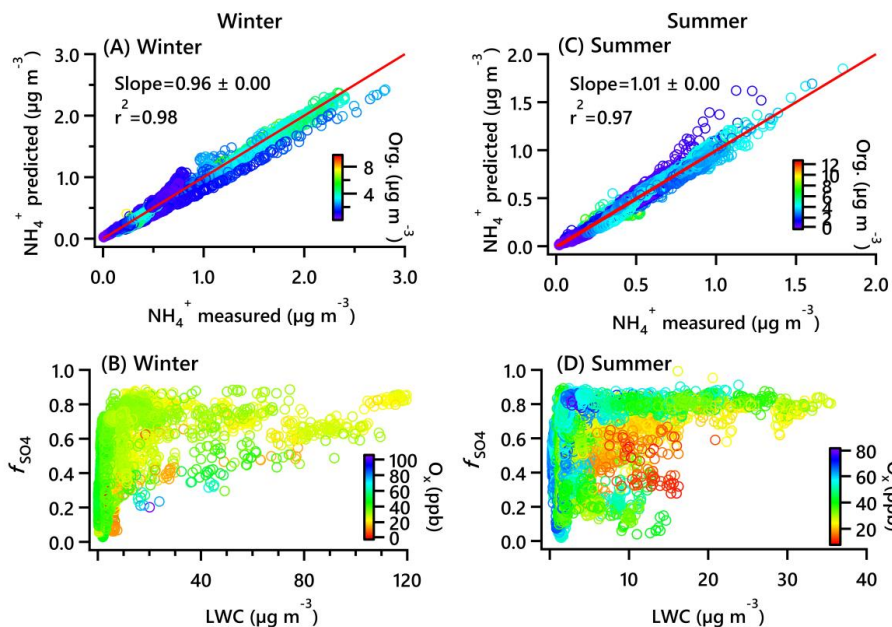
Figure 3. (A, C) Scatterplots of predicted NH$_4^+$ vs. measured NH$_4^+$ concentrations over the winter and summer campaigns. The predicted values were estimated assuming full neutralization of the HR-ToF-AMS-measured SO$_4^{2-}$, inorganic NO$_3^-$ and Cl$^-$. The data points were colored by organic concentrations, and the red line is the 1:1 relationship. **(B, D)** Scatterplots of f_{SO4} vs. LWC, with data points colored by O$_x$ concentrations over the winter and summer campaigns.

Atmospheric
Chemistry
and Physics
Discussions
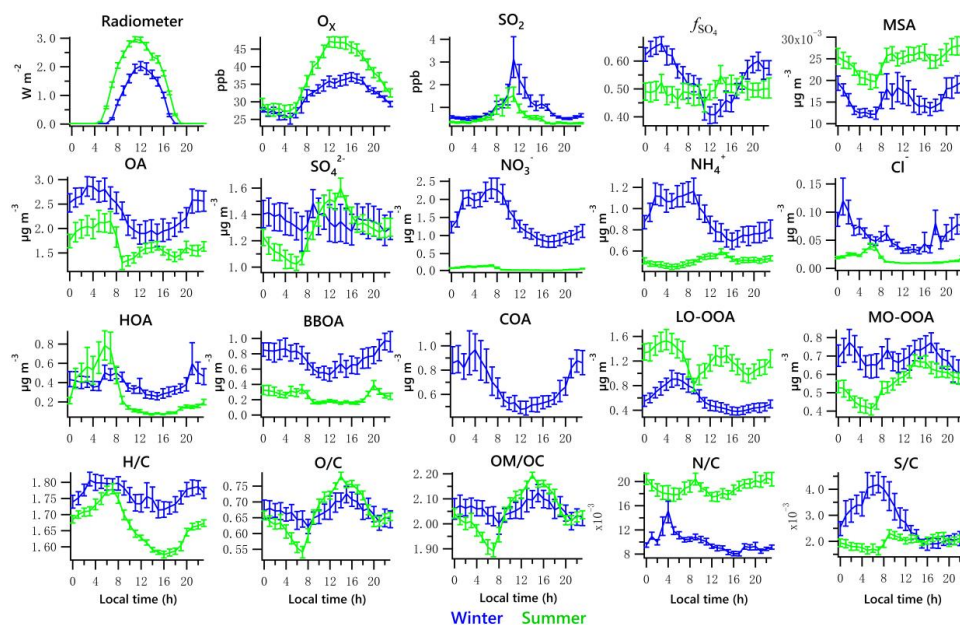
Figure 4. Diurnal profiles of radiometer, O_x, SO_2, f_{SO4}, MSA, each of the five NR-PM$_1$ species (Org, SO_4^{2-}, NO_3^-, NH_4^+ and Cl^-), PMF-resolved factors (HOA, BBOA, COA, LO-OOA and MO-OOA) and elemental ratios (H/C, O/C, OM/OC, N/C and S/C). Lines denote the mean value, and bars represent the 5/95 percent confidence interval in the mean (blue for winter, green for summer).
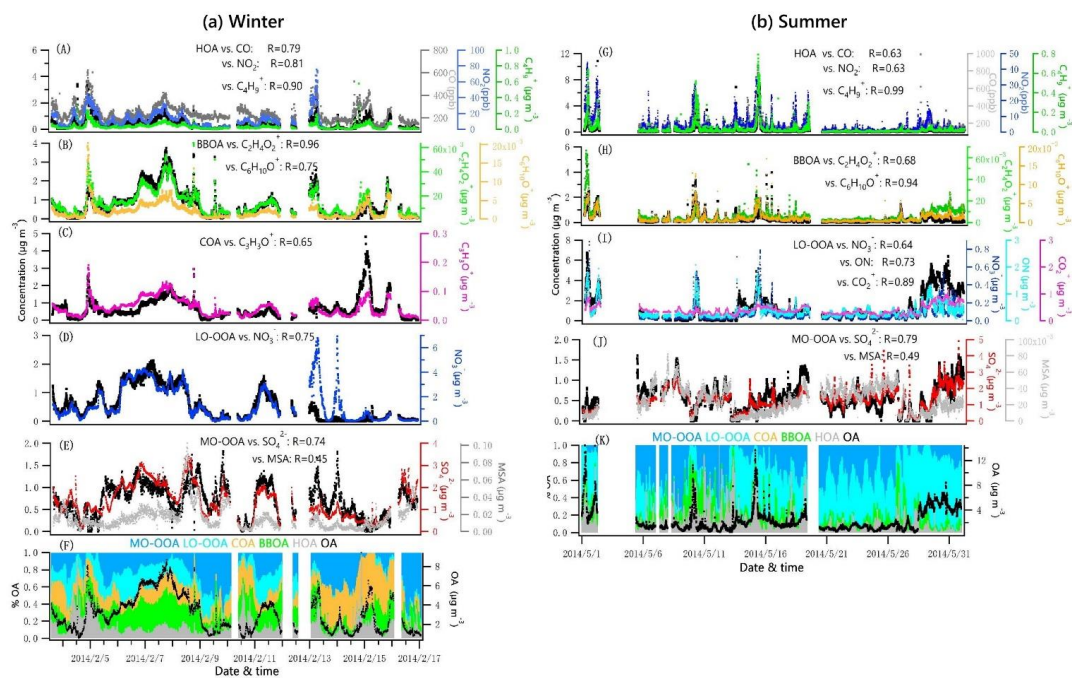
Figure 5. Time series of each OA factor and associated correlated species for the winter and summer campaign at UHSL.
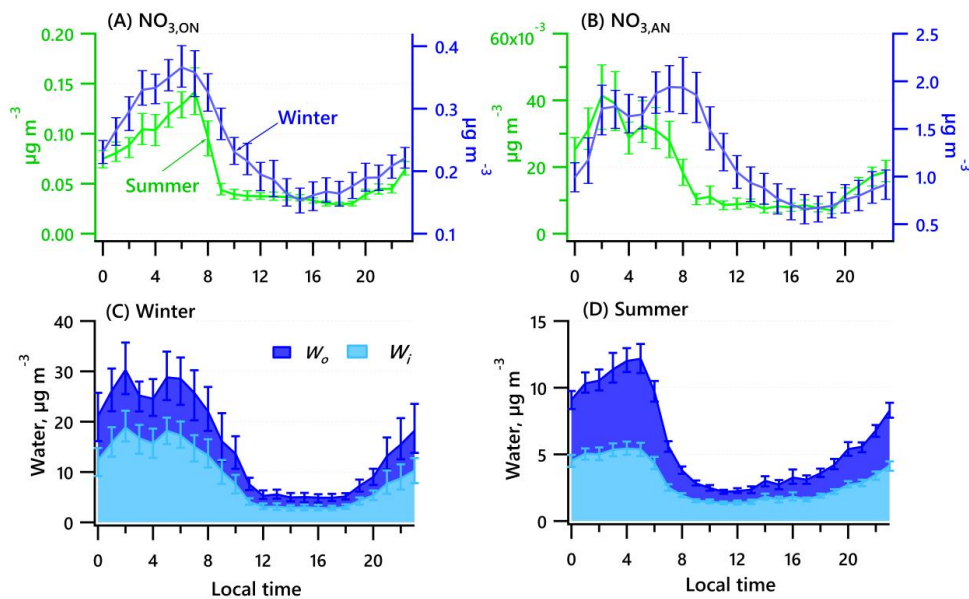
Figure 6. Diurnal profiles of nitrate functionality from organic nitrate (**A**) and inorganic nitrate (**B**) for the winter and summer campaigns. Estimated water associated with inorganic and organic aerosol for the winter (**C**) and summer campaigns (**D**). Solid lines denote the mean value (blue for winter, green for summer), and bars represent the 5/95 percent confidence interval in the mean.

1039
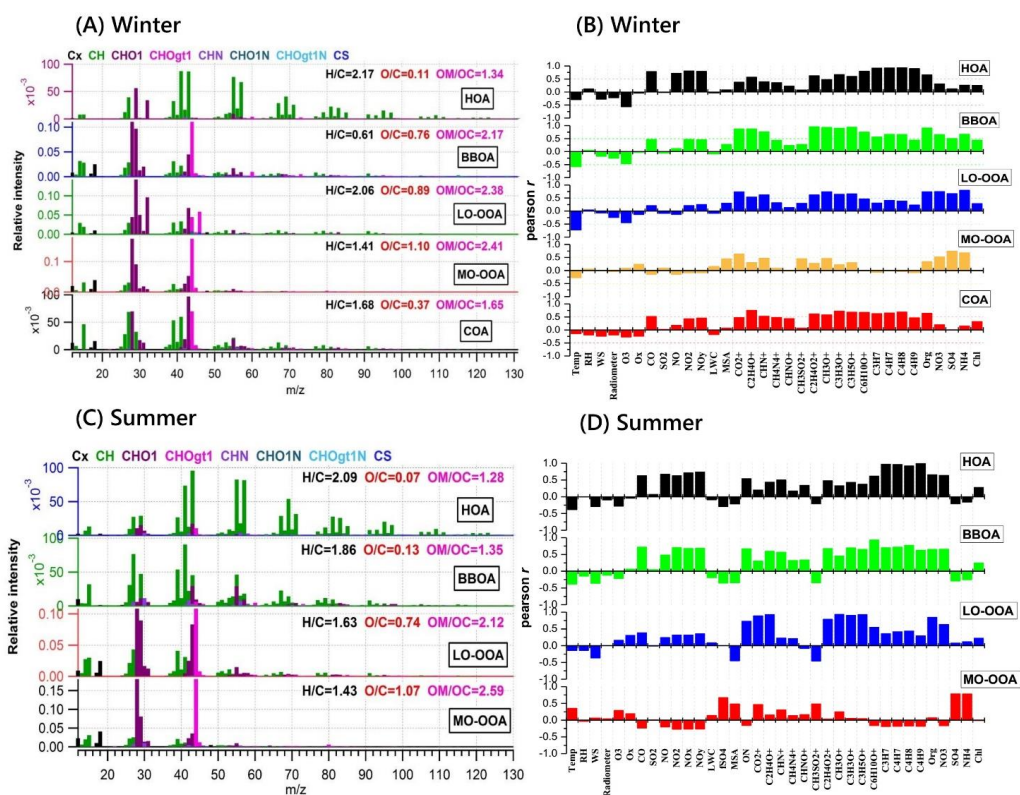
1040

Figure 7. Mass spectra of PMF-resolved OA factors (**A**, **C**) and correlation coefficients between OA factors and other variables (tracer ions, trace gas, meteorological parameters, etc.) (**B**, **D**) for winter and summer campaigns at UHSL.
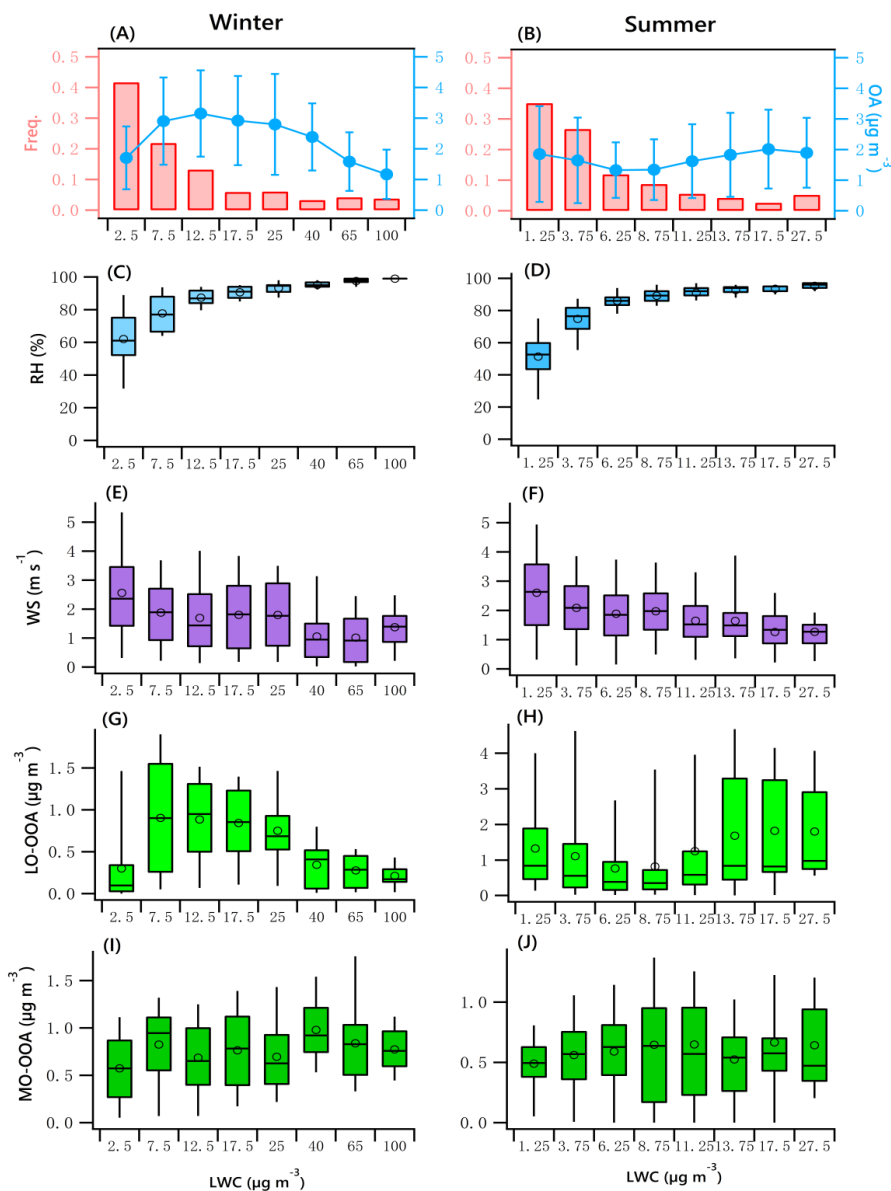
Figure 8. OA mass and frequency histograms of data points in each LWC bin for winter (**A**) and summer (**B**). Variations of RH, WS, LO-OOA and MO-OOA mass as a function of LWC in winter (**C, E, G, I**) and summer (**D, F, H, J**). The data were binned according to the LWC (with different increment values), and mean (circle), median (horizontal line), 25th and 75th percentiles (lower and upper box), and 5th and 95th percentiles (lower and upper whiskers) are displayed for data in each bin.
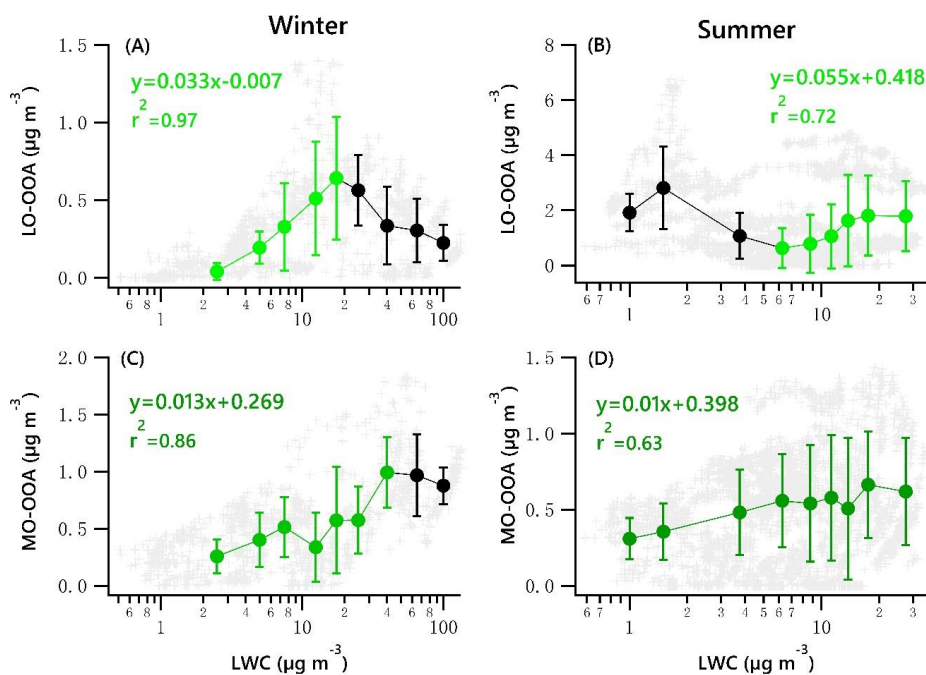
Figure 9. Scatter plots of nighttime OOA vs. LWC for the winter and summer campaign. The linear equations are given for fitting only the green dots. Solid dots denote the average value of data in each bin. Bars indicate standard deviations.
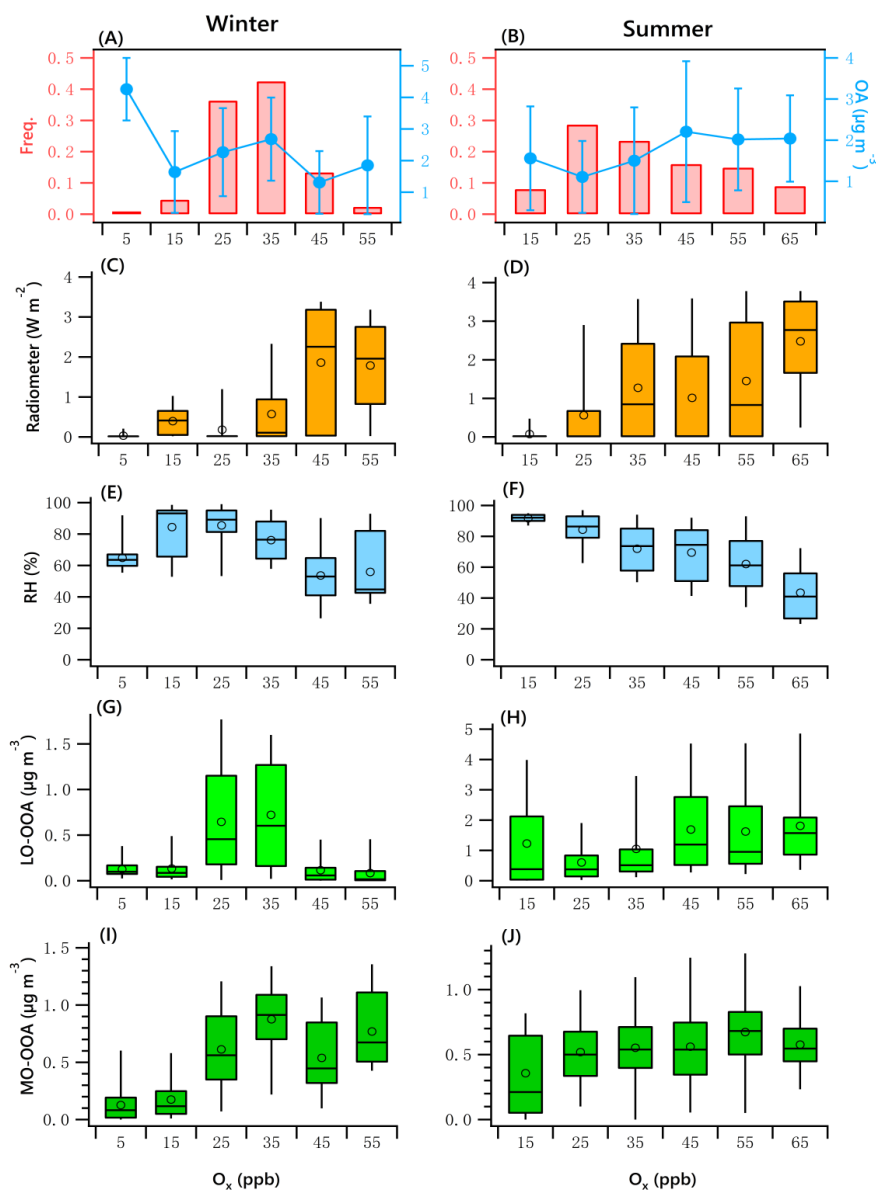
Figure 10. OA mass and frequency histograms of data points in each O_x bin for winter (**A**) and summer (**B**). Variations of solar radiation, RH, LO-OOA and MO-OOA mass as a function of LWC in winter (**C, E, G, I**) and summer (**D, F, H, J**). The data were binned according to the O_x (10 ppb increment), and mean (circle), median (horizontal line), 25th and 75th percentiles (lower and upper box), and 5th and 95th percentiles (lower and upper whiskers) are displayed for data in each bin.
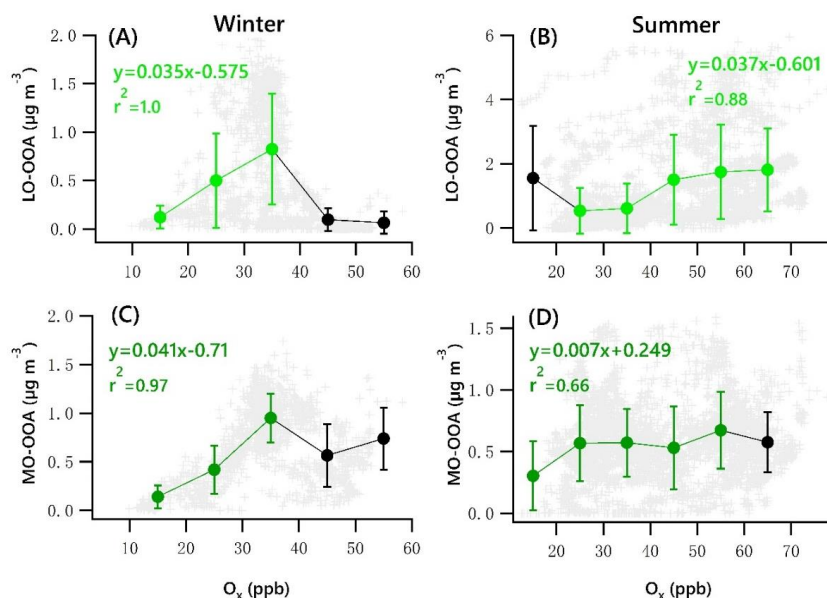
Figure 11. Scatter plots of daytime OOA vs. O_x for the winter and summer campaign. The linear equations are given for fitting the green dots. Bars indicate standard deviations.
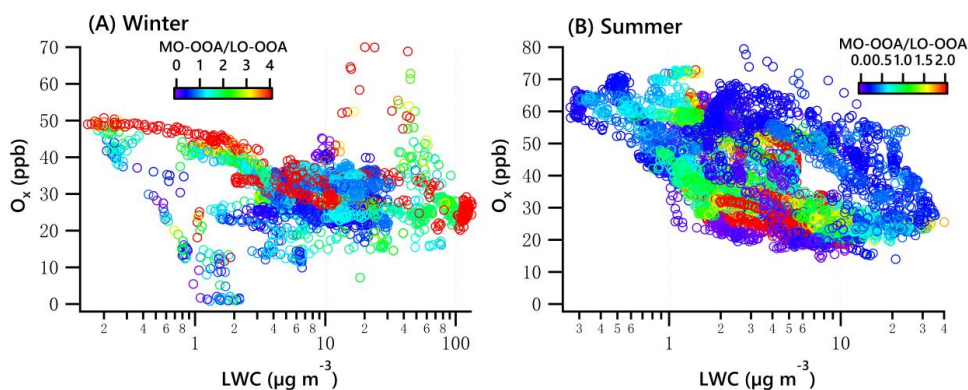

Figure 12. O_x vs LWC dependence of the ratio of MO-OOA/LO-OOA in winter (**A**) and summer (**B**).